AN OPERATOR-BASED APPROACH TO UPSCALING THE PRESSURE EQUATION

TODD ARBOGAST, SUSAN MINKOFF, AND PHIL KEENAN *
CENTER FOR SUBSURFACE MODELING,
TEXAS INSTITUTE FOR COMPUTATIONAL AND APPLIED MATHEMATICS
TAYLOR HALL 2.400; C0200,
UNIVERSITY OF TEXAS, AUSTIN, TEXAS 78712

Abstract. The input permeability and porosity fields which describe a reservoir are uncertain. Generally only statistical information is known about the distribution of these parameters over the whole field. For risk assessment, one must perform multiple flow simulations of a single field, varying these input parameters. Because multiple simulations of realistic-sized fields are computationally prohibitive, reservoir engineers scale up the numerical grid and consequently the permeability and porosity fields. In this paper we advocate determining a new coarse grid operator which provides an upscaled solution but bypasses determination of an effective or upscaled permeability field. The method requires that we solve the upscaled problem in two steps. We first solve for fine scale flow information internal to each coarse grid block. Then we determine a *modified* coarse grid operator for solving the upscaled problem which includes the fine scale flow information from the first step. The method is developed for the single-phase pressure equation in the context of the mixed finite element method and is, therefore, locally mass conservative. Using operator-based upscaling we never solve for all the fine grid unknowns. As the ratio of fine to coarse grid blocks increases, the computational cost decreases. Unlike traditional upscaling methods (homogenization) we do not impose arbitrary boundary conditions on the coarse grid. We test the method against two traditional upscaling techniques on three permeability fields. In the first case we apply the method to a high-permeability streak diagonal to the direction of flow. Only operator-based upscaling qualitatively captures the correct fine scale behavior. Our method also does the best of the three methods when the global domain has nonstandard boundary conditions. Finally, the method accurately captures local information about flow trapped by shale barriers.

Key words. Upscaling, mixed finite element method, reservoir simulation

*NOW AT MCKINSEY AND ASSOCIATES

1. Introduction. Modeling of physical systems requires input data which may have significance on many different spatial scales. As an example, in this paper we will be concerned with simulating the flow of fluids through an oil reservoir. Permeability and porosity fields are required as input for even the simplest reservoir simulation models. The engineer makes core sample measurements of both these fields. However, the measurements are made at the wells which leads to very fine resolution vertically (3 inches) and very coarse resolution in the horizontal directions (thousands of feet) [17]. He then generates geostatistics based on this limited information to allow extrapolation away from the wells. (For an example see the paper by Dimitrakopoulos and Desbarats [6].) Thus, he ends up with a very finely resolved description of very uncertain parameters.

For risk assessment, the engineer runs a number of flow simulations varying the input parameter distribution drawn from the limited geostatistical information. Running a number of fairly detailed reservoir simulations is usually not computationally feasible in reasonable time. Thus, the engineer is forced to work with a coarser description of the input parameters. *Upscaling* is the process of redefining (averaging) the physical system's parameters *up to* a coarser grid. Engineers refer to these new parameters as *effective or equivalent* parameters, see [8].

Upscaling for both single and multiphase flow simulation is currently a very active area of research. For single-phase flow, the simplest and cheapest methods are arithmetic and harmonic averaging of the fine grid parameter fields. Amazingly, even for these very simple methods, little is known about the accuracy of the resulting coarse-grid flow simulations. An attempt to analyze the upscaling error appeared in in the paper by King and Williams [16]. These types of averaging seem most reliable when the directions of preferential flow (high permeability) are parallel to the coordinate directions, and when the correlation lengths of the permeability heterogeneity are small compared with the size of the coarse grid blocks [8]. Simple averaging, although clearly incorrect in certain well-documented situations (see Experiment 1 in Section 4.2) is nonetheless the most common upscaling technique.

Another common upscaling idea is the pressure solver method. The engineer runs a fine grid flow simulation (imposing arbitrary boundary conditions) and calculates the net flow through each coarse block. (The most common boundary conditions are no flow on the top and bottom and a unit pressure drop from left to right across the grid block.) He then determines a single number (or effective permeability) K_{eff} for each coarse block which produces the same net flow through the block as the flow simulation on the fine grid. The resulting coarse grid permeability field is subsequently used for upscaled flow simulation. Although this method is more accurate than simple harmonic averaging in some situations, the arbitrary boundary conditions imposed on each coarse grid block have a very large influence on the resulting upscaled solution. (For examples of the pressure solver method see the paper by Christie [4].)

Homogenization, a third upscaling method, has been studied rigorously by Bensoussan et al. [1], Bourgeat [2], Arbogast (?), and E [11]. The idea is that we assume the medium under study depends on two separate spatial scales denoted x and y. For the elliptic pressure equation, let a denote the permeability coefficient which characterizes the medium. Then we write $a = a(y) = a(x/\epsilon)$, where ϵ characterizes the small scale of the problem. Homogenization theory states that if we write the solution to our equation via an asymptotic expansion $u = u_0(x) + \epsilon u_1(x, y) - \epsilon\theta_\epsilon + O(\epsilon^2)$ where $y = x/\epsilon$ is the fast variable, then u_0 solves the homogenized pressure equation

$\nabla \cdot a^* \nabla u_0 = f$ in Ω. Here a^* is the constant effective coefficient (see Hou and Wu [13]). Homogenization relies on two key assumptions (see [8]):

1. Two distinct scales of the coefficient variation exist. Equivalently, the scale of the effective permeability is large compared to the correlation length of the heterogeneity within the porous medium.

2. The medium and its boundary conditions are periodic.

Hou and Wu [13] rigorously analyze a closely-related method, the multiscale finite element method. Specifically they show that the method produces results consistent with those of traditional finite element methods for fine scale simulations. In addition, they have added "over-sampling" to allow relaxation of assumption 1 above.

Another popular upscaling idea is renormalization [15]. In renormalization, one uses simple upscaling ideas like harmonic averaging and the pressure solver approach to successively solve the problem on coarser and coarser (nested) grids. The idea is that by upscaling in stages (for example, upscale from a 100x100 $\rightarrow$ 50x50 grid and then from a 50x50 $\rightarrow$ 25x25 grid rather than from a 100x100 $\rightarrow$ 25x25 grid directly), one can capture different length scales in the final coarse-gridded solution. In truth, there appears to be little evidence supporting this claim. Numerical experiments indicate that the accuracy of the renormalized solution on the coarse grid is almost identical to the solution gotten from upscaling in a single step. However, the total cost of upscaling is reduced in the renormalization method.

Other areas of active research for upscaling the single-phase pressure equation include multigrid methods [18], finite difference support operators [14], and wavelet bases [12].

For multiphase flow, the upscaling methods are more complex as it is no longer enough to find a new effective absolute permeability field. Effective *relative permeabilities* are also important in order to capture the global flow behavior, breakthrough times, and post-breakthrough fractional flows of all reservoir fluids. Methods of upscaling for multiphase flow include nonuniform coarsening of the reservoir by targeting high-flow regions for finer resolution [10, 9] and renormalization [17, 5].

In this paper we describe a method which is fundamentally different from the other upscaling methods described above because *no new effective coefficients* (permeability and porosity) are defined on the coarse grid. *Instead we define an effective solution* (pressure and velocity) directly. The main idea is to solve the problem in two stages using the mixed finite element method. First solve for the fine-scale unknowns internal to each coarse grid block. Each of these small problems may be solved independently. Then use these solutions to redefine the coarse grid (upscaled) problem to be solved. The original fine grid permeability field (and fine grid numerical quadrature) are used throughout both stages. The advantages of the method over the upscaling methods described above are

- The method has been developed in the context of the mixed finite element method, and should therefore be amenable to error analysis. Moreover, the mixed finite element method maintains local conservation of mass.

- The original physical boundary conditions are used to solve the upscaled problem.

- The method is cheaper than solving the original full fine grid problem as we do not solve for the full set of fine grid unknowns.

- The solution is at least as accurate as solving the problem on the coarse grid directly.

To simplify calculations, all of our numerical examples were performed on the single-phase, incompressible pressure equation in two dimensions. The permeability field is assumed to be diagonal and discontinuous. We compare the method to two other standard techniques — harmonic averaging and the pressure solver approach — on three different permeability fields. Both of the two standard methods calculate a new effective permeability field on the coarse grid. Our approach does not. The first numerical example indicates the superiority of the method for the difficult case of a high permeability streak diagonal to the direction of flow. It is clear that allowing for a more complicated non-diagonal tensor permeability would improve the results further. Examples 2 and 3 indicate that when we impose non-standard boundary conditions on the physical domain, the operator-based approach gives more accurate answers than either harmonic averaging or the pressure solver method. The latter two methods do not use the original domain boundary conditions when determining the effective permeabilities. Finally, Example 3 indicates that of the three methods, only the new upscaling approach captures local information about flow trapped by shale barriers and other complicated geologies.

Section 2 of this paper describes the new operator-based upscaling method in the context of the mixed finite element method (MFEM). In Section 3 we describe the numerical implementation of the method, and in Section 4 we give several numerical examples. Finally Section 5 is a discussion of the current results and future directions for the work.

2. The Method.

2.1. The Pressure Equation and Mixed Finite Element Method. By combining Darcy's Law with conservation of mass we arrive at the pressure equation for single phase flow. Let Ω be a domain in $\Re^d$, $d = 1, 2, 3$ with boundary Γ. We solve simultaneously for the pressure p in the center of the grid blocks and velocity u on the interfaces of the cells. To illustrate the MFEM formulation, we write the elliptic pressure equation as

$$\begin{cases} -K\nabla p = u & \text{in } \Omega \\ \phi p + \nabla \cdot u = q & \text{in } \Omega \end{cases} \tag{2.1}$$

Here $\phi(x, y)$ = is related to rock compressibility (or equivalently, porosity). The permeability $K(x, y)$ is assumed to be discontinuous and diagonal on each fine grid block. The source term is $q(x, y)$, and ν is the unit outward normal. For the set of equations to be well-defined, we must specify conditions on the boundary Γ of the domain. Let

$$\begin{cases} p = g^D & \text{on } \Gamma^D \\ u \cdot \nu = g^N & \text{on } \Gamma^N \end{cases} \tag{2.2}$$

Here Γ^D is the portion of the boundary with imposed Dirichlet conditions, g^D, and Γ^N the portion with Neumann boundary conditions, g^N. Writing the system in variational form and integrating by parts, we solve the following mixed finite element system for velocity $u \in V$ and pressure $p \in W$:

$$\begin{cases} (K^{-1}u, v) - (p, \nabla \cdot v) = -\langle g^D, v \cdot \nu \rangle, \\ (\phi p, w) + (\nabla \cdot u, w) = (q, w), \\ \langle u \cdot \nu, \mu \rangle = \langle g^N, \mu \rangle \end{cases} \tag{2.3}$$

The L^2 inner product on the boundary of the domain is denoted $\langle \cdot, \cdot \rangle$ and on the interior by $(\cdot, \cdot)$. V is the basis function space for velocity, and W is the function space for pressure. Specifically,

$$\begin{aligned} & v \in V = H(div; \Omega) = \{v \in L^2(\Omega)^2 : divv \in L^2(\Omega)\}, \\ & w \in W = L^2(\Omega) \end{aligned} \tag{2.4}$$

The name *mixed method* indicates that we find a finite-dimensional approximation space for *both* the pressure and the velocity simultaneously. For details of the MFEM see the paper by Douglas and Roberts [7] and the book by Brenner and Scott [3].

2.2. Operator-Based Upscaling. Idea: Decompose the fine scale unknowns (velocity and pressure) into a coarse piece and perturbational remainder. Let V, W be the function spaces for velocity and pressure on the full fine grid, and let V_c and W_c be the mixed spaces on the coarse grid. Our goal is to capture some of the fine grid flow internal to each coarse block without solving the full fine grid problem. To achieve this aim, we rename the subset of the fine grid unknowns internal to each coarse grid block as δ-*problem* unknowns. The function spaces for these unknowns will be denoted δV and δW. Moreover, we assume that:

$$\begin{cases} V = V_c + \delta V \\ \delta V = \{\delta v \in V : \langle \delta v \cdot \nu, 1 \rangle_{e_c} = 0\} \end{cases} \tag{2.5}$$

$$\begin{cases} W = W_c \oplus \delta W \\ \delta W = \{\delta w \in W : (\delta w, w_c) = 0\} \end{cases} \tag{2.6}$$

The first line in equations 2.5 and 2.6 defines the decomposition of the velocity and pressure spaces into a set of unknowns on the coarse grid and a set on the fine grid. For pressure we assume that the coarse and δ-function spaces are orthogonal.

We will solve a δ-problem on each coarse grid block (i.e., solve for internal fine grid unknowns). Line 2 of equation 2.5 is the only restrictive simplifying assumption

in the definition of the method. This *closure assumption* states that we impose homogeneous Neumann boundary conditions on the δ-problems. It allows us to decouple the δ-problems from coarse grid block to coarse grid block and would make a parallel implementation of the method straight-forward. (We do not discuss such an implementation in this paper.) *Note, however, that we are not imposing arbitrary boundary conditions on the the final upscaled problem.* We could make other closure assumptions as well. For example, we could assume that the δ-problem velocity unknowns are discontinuous on the coarse grid block edges. However, at present, we have only investigated the closure assumption given in equation 2.5 above.

We define two projections which are important to the description of the MFEM and this upscaling technique in particular. Recall from [3, page 52] that

DEFINITION 1. *An operator P on a linear space V is a projection if $P^2 = P$, i.e., $Pz = z$ for all z in the image of P.*

The L^2 projection P of the function u is defined over the whole domain Ω (a global quantity) and is given by

$$\int_\Omega (Pu - u) \cdot v = 0 \tag{2.7}$$

The π-projection of u is the average of the normal component of u. In contrast to the L^2 projection, the π-projection is a local quantity which preserves continuity of fluxes and is defined over a grid block edge e via

$$\frac{1}{|e|} \int_e (\pi u - u) \cdot v = 0 \tag{2.8}$$

Rewriting equation 2.5 (line 1) in terms of functions rather than spaces we see from 2.8 that if $u \in V$ and $\pi_c : V \to V_c$ then

$$u = \underbrace{\pi_c u}_{u_c} + \delta u \tag{2.9}$$

Similarly, assuming $p \in W$ and $P_c : W \to W_c$, equation 2.6 (line 1) can be rewritten for functions via the projection 2.7:

$$p = \underbrace{P_c p}_{p_c} \oplus \delta p \tag{2.10}$$

Now substituting the quantities $u = u_c + \delta u$ and $p = p_c + \delta p$ back into the variational system, Equation 2.3, we recover two sets of problems to solve: **First, on each coarse grid block we solve one (small) δ-problem:** find $\delta u = \delta u(p_c, u_c) \in \delta V$ and $\delta p = \delta p(p_c, u_c) \in \delta W$ such that

$$\begin{cases} (K^{-1}(u_c + \delta u), \delta v) - (\delta p, \nabla \cdot \delta v) = 0 \\ (\phi(p_c + \delta p), \delta w) + (\nabla \cdot \delta u, \delta w) = (q, \delta w) \end{cases} \tag{2.11}$$

Because we do not know the values of u_c and p_c at this stage, these terms act as sources (forcing terms) for the δ-problems. The δ-pressure solution is computed by the sum

$$\delta p = \delta p_0 + \sum_{l=1}^{4} u_{cl}\delta p_l + p_c \delta p_5 \tag{2.12}$$

Where the u_c are coarse grid velocity basis functions (one for each edge of the coarse block) and p_c is the coarse grid basis function for pressure. The remaining terms in Expression 2.12 are coefficients. The first term in the sum (Equation 2.12) is the solution to the problem forced by q, the physical source term. The δ-velocity solution is determined by a similar sum of six solutions.

The second step of the upscaling process is to **use the δ-problem solutions, δu and δp, to form the Coarse Problem:**

$$\begin{cases} (K^{-1}(u_c + \delta u), v_c) - (p_c, \nabla \cdot v_c) = -\langle g^D, v_c \cdot \nu \rangle \\ (\phi(p_c + \delta p), w_c) + (\nabla \cdot u_c, w_c) = (q, w_c) \\ \langle u_c \cdot \nu, \mu_c \rangle = \langle g^N, \mu_c \rangle \end{cases} \tag{2.13}$$

We have found a new coarse-grid linear operator $\mathcal{L}(u_c, p_c) = K^{-1}(u_c + \delta u(u_c, p_c))$, rather than a new value for K. We, therefore, refer to this new method as **operator-based upscaling**.

3. Numerical implementation. To approximate the solution to equations 2.11 and 2.13, we define finite-dimensional function spaces V_h, W_h for both the small δ-problems and the upscaled problem. For our numerical implementation, we chose the lowest-order Raviart Thomas spaces (see paper [20]). Namely, the velocity spaces contain continuous linears and the pressure spaces piecewise discontinuous constant elements. One must be careful to ensure orthogonality of the δ and upscaled pressure spaces (see Eqn. 2.6). If E is a rectangular element on either the fine or coarse scale, then

$$V_h(E) = \{(\alpha_1 x_1 + \beta_1, \alpha_2 x_2 + \beta_2)^T : \alpha_i, \beta_i \in \Re\}$$
$$W_h(E) = \{\alpha : \alpha \in \Re\}$$

We solve for velocity unknowns defined in the middle of the cell block edges and for pressure unknowns in the cell centers. Recall that the closure assumption (Line 2, Eqn. 2.5) takes care of the boundary conditions for the δ-problems. To correctly handle the boundary conditions for the upscaled problem, we introduce Lagrange multiplier pressures at the midpoints of the cell edges. Thus, for a coarse grid edge e, we define the space

$$\Lambda_h(e) = \{\alpha : \alpha \in \Re\}.$$

Having modified the elliptic operator in this upscaling process (see Eqn. 2.13), we no longer can assume that the lowest-order Raviart-Thomas mixed method will be equivalent to cell-centered finite differences on this problem. (Without upscaling, the two techniques are equivalent [21] if one assumes a diagonal permeability matrix as in this implementation.) Instead, we use exact quadrature and evaluate the finite element integrals directly. We used Simpson's quadrature rule for the velocity integrals, and the midpoint rule for the pressure integrals.

Even for a small problem, the linear system is prohibitively large. Thus, we took two steps towards minimizing the memory needed to solve this problem. First, we rewrote the system in terms of its Schur complement and actually solve the linear system for Lagrange multiplier pressure unknowns only. We then back out the velocities and cell-center pressures from the Lagrange multiplier pressure solutions and equations relating the three sets of unknowns. Second, we store the linear system in a sparse matrix format and use the UT Center for Numerical Analysis iterative package *NSPCG*. For a description of the NSPCG package see [19].

4. Numerical Experiments.

4.1. Upscaling comparisons: other methods, error calculation. In this section we apply three types of upscaling to a set of permeability fields. Two of the upscaling methods (harmonic averaging and the pressure-solver approach) require that we determine a new coarse-grid effective permeability field for upscaling. The third method (operator-based upscaling) does not require a new permeability field be defined on the coarse grid. Instead, the original fine grid permeability field is used even for the coarse grid simulation.

All the numerical experiments described in this paper were performed using the same pressure equation MFEM code (see Section 3 for details). In the case of harmonic averaging, we determine a new permeability field in the following way. Assume that we are upscaling from a 2x1 fine grid block to a 1x1 block. Let k_x^- denote the permeability on the left block of the fine grid, and k_x^+ the permeability on the right block. Similarly, h_x^- is the size of the left block (width in x) and h_x^+ the size of the right block. Then, the harmonic-average effective permeability value for the single coarse grid block k_x^H is given by:

$$k_x^H = \left(\frac{h_x^-/k_x^- + h_x^+/k_x^+}{h_x^- + h_x^+} \right)^{-1} \tag{4.1}$$

The effective permeability in the y-direction k_y^H is calculated similarly. Clearly, if we combine more than two fine grid blocks to form a single coarse block, then we must sum over all fine grid blocks in equation 4.1 appropriately. After calculating the effective permeability values (one k_x and one k_y per coarse grid block), we then run the flow simulation with this upscaled permeability field to determine an upscaled solution.

An alternate but similar upscaling idea is the pressure solver method. We simulate fine-grid flow through each coarse grid block of the domain. The most common boundary conditions for the coarse block simulations are no flow on the top and bottom edges of the domain and a unit pressure drop across the domain. Again, we

compute a single effective (k_x,k_y) permeability pair for each coarse block by matching the flow through that block to the flow through the fine blocks which make up the coarse block. If one assumes standard boundary conditions, the resulting effective permeability tensor will be diagonal. Alternatively, one may assume periodic boundary conditions. However, then the effective permeability is a more complicated full tensor (see [4]). As in the case of harmonic-average upscaling, after calculating a new effective permeability field, we solve the upscaled problem by running a flow simulation on the coarse grid.

Table 4.1 gives velocity and pressure errors calculated for all the experiments using the three different upscaling methods: harmonic averaging, pressure solver, and operator-based upscaling. To calculate the errors in the upscaled solutions, we assume that the best upscaled solution comes from solving the full fine grid problem and then *projecting* that solution onto the coarse grid. We calculate the relative norm error in the upscaled pressure by:

$$\frac{||P_c p - p_u||}{||P_c p||}$$

Here we take $||\cdot||$ to be the L^2 norm. $P_c p$ is the L^2 projection of the fine grid pressure solution onto the coarse grid, and p_u is the coarse grid pressure calculated using one of the three upscaling methods. Similarly, we calculate the relative norm error in the upscaled velocity by:

$$\frac{||\pi_c u - u_u||}{||\pi_c u||}$$

Here $\pi_c u$ is the π-projection of the fine grid velocity solution onto the coarse grid, and u_u is the coarse grid velocity calculated using one of the three upscaling methods. (In Table 4.1 we used the L^1 norm for the velocity error. However, we could just as easily have computed the L^2 norm for velocity as well as pressure.)

The discrete pressure projection $P_c p$ is calculated by summing the fine scale pressure solutions for each coarse grid block and weighting by the volume of the fine grid blocks. In other words, if $n\delta x$ and $n\delta y$ are the number of fine grid blocks in the x and y directions respectively for a particular coarse grid block, and if h_x and h_y denote the fine grid block widths, then

$$P_c p = \frac{\sum_{i=1}^{n\delta x} \sum_{j=1}^{n\delta y} p(i,j) h_x(i) h_y(j)}{\sum_{i=1}^{n\delta x} \sum_{j=1}^{n\delta y} h_x(i) h_y(j)} \tag{4.2}$$

Similarly we calculate the π-projection for velocity. We only sum over velocity components on the coarse block edges (since the velocity unknowns are defined on cell edges). If e_c is a particular vertical coarse block edge, we calculate the projection of the x-component of velocity on that edge via:

$$\pi_c u_x = \frac{\sum_{i \in e_c} u_x(i) h_y(i)}{\sum_{i \in e_c} h_y(i)} \tag{4.3}$$

A similar calculation allows us to compute the projection from the fine to the coarse grids of the y-component of velocity. Figure 5.2 shows these two projected solutions schematically assuming we are upscaling from 4 fine grid blocks to a single coarse block.

4.2. Discussion of results. All of the numerical experiments discussed in this paper are summarized in Table 4.1. We break the experiments into three groups (Experiments 1–3) for each of the three different permeability fields studied. For each of these permeability fields, we ran from 1-3 subcases in which we varied the size of the upscaled grid or the boundary conditions. The boundary conditions are labeled either "S" for *standard* or "NS" for *nonstandard*. The two sets of boundary conditions are shown in Figure 5.1.

For the first permeability field, we describe only one subcase as other cases we ran provided qualitatively similar results (for example, varying the boundary conditions). The fine grid permeability field for this example has a high-value streak diagonal to the direction of fluid flow. We assume the standard boundary conditions. The permeability throughout the domain is taken to be 1 mD except along the diagonal streak where it has value of 1000 mD (see Figure 5.3). (Note that the plotting package averages contour color levels in the Figure legend.) This example is traditionally difficult for standard upscaling methods, and although somewhat unrealistic as a description of the entire permeability field, this example would realistically be a *component* in many reservoirs formed by dipping beds and faulting. It is therefore an important example to study. The full fine-grid (40x40) solution is shown in Figure 5.4. Each solution plot shows both the color pressure contours and velocity vectors. The figures are intended to give mainly information about the quality of the solution. Numerical errors for all experiments are given in Table 4.1.

Because our method for solving the pressure equation did not include a full tensor permeability matrix, it is not surprising that *quantitatively*, none of the methods accurately capture the high velocity values along the diagonal streak (see Table 4.1, Expt.1). Nonetheless, two important observations can be made about this example. First, while the harmonic-average upscaled solution captures the basic characteristics of the fine grid pressure field, it does *not* at all reproduce the correct velocity vector directions (see Figure 5.5). In fact, the velocity vectors seem no longer to be influenced by the diagonal streak. Rather, they run parallel to the top and bottom edges of the grid. In contrast, the pressure-solver upscaled solution does a much better job of capturing the correct velocity direction, but achieves this end by skewing the upscaled pressure field (Figure 5.6). Only the operator-based upscaled solution qualitatively captures the correct velocity vector direction and the correct upscaled pressure (Figure 5.7).

The fine grid permeability field for Example 2 is a two-dimensional slice (see Figure 5.8) taken from a 3-dimensional (32x32x32) permeability cube. The permeability is described in reference [5] (where it is called "Case 6"). The permeability cube is log-normally distributed with mean 5.0 and standard deviation 1.0. Permeability values fall primarily in the range from 20-1000 mD. For this permeability field we ran three subcases (see table 4.1). In Subcase 1 we upscaled from a fine grid of 32x32 to a coarse grid of size 16x16. In Subcase 2 we upscaled the original domain to a coarse grid of size 8x8. In both Subcases 1 and 2 the domain boundary conditions were standard. In Subcase 3 we also upscaled to an 8x8 coarse grid, but we applied nonstandard boundary conditions to the original grid. Because the results are quali-

tatively very similar, we do not show all the upscaled solutions for these subcases. We show the full fine grid solution (assuming standard boundary conditions) in Figure 5.9. The full fine grid solution (assuming nonstandard boundary conditions) is displayed in Figure 5.13. Figure 5.10 shows the operator-based upscaled solution on the 16x16 coarse grid with standard boundary conditions (Subcase 1). Figure 5.12 shows the operator-based upscaled solution on the 8x8 coarse grid with standard boundary conditions (Subcase 2), and Figure 5.14 shows the operator-based upscaled solution on the 8x8 coarse grid with non-standard boundary conditions (Subcase 3). For this permeability field, the three upscaling methods give fairly comparable results although the operator-based approach does a better job in both pressure and velocity when the boundary conditions are non-standard (see Subcase 3, Table 4.1). For comparison, the projection of the fine solution to the 8x8 coarse grid is plotted for Subcase 2 in Figure 5.11.

We see a similar phenomenon in the last example (Example 3). This 128x128 permeability field realistically describes geologically thin, flat layers (i.e., shales). These low-permeability regions act as barriers to flow upward through the domain. The permeability field for the fine grid is shown in Figure 5.15. The full fine grid solution with standard boundary conditions is shown in Figure 5.16. Subcase 1 involves upscaling this problem to a grid of size 16x16 assuming the standard boundary conditions. Strangely, the operator-based upscaling method does not give accurate results in this case. The pressure front does not advance as far as it should into the domain. The velocity vectors also are too small. The operator-based upscaled solution is shown in Figure 5.20. Results from the other two upscaling methods are shown in Figures 5.18 and 5.19. For comparison, the projection of the fine solution to the coarse grid (used in calculating the errors in Table 4.1) is plotted in Figure 5.17. Clearly, the harmonic-average and pressure-solver upscaling methods are closer to the projected fine grid solution than is the operator-based approach in this case. Subcases 2 and 3 involve upscaling from the fine grid to a 16x16 coarse grid and also to an 8x8 coarse grid using non-standard boundary conditions. As with Example 2 discussed above, the operator-based approach does qualitatively and quantitatively better in these cases. The full fine grid solution is shown in Figure 5.21. The operator-based upscaled solution on the 16x16 coarse grid is shown in Figure 5.22. Figure 5.23 gives the projection of the fine grid solution to the coarse 8x8 grid. One notices that the low-permeability shale barriers only allow fluid to flow in the lower left corner of the domain. However, the harmonic-average and pressure-solver upscaled solutions have smeared the pressure front, and we see inflow of fluid along the whole bottom edge of the grids (see Figures 5.24 and 5.25). In contrast, the operator-based approach has done a good job of capturing that fine scale trapped flow (see Figure 5.26). One also notes that the other pressure contours are more accurate in the operator-based solution.

5. Conclusions. In this paper we present a method for upscaling which is fundamentally different from traditional upscaling techniques in that we do not produce a new effective input parameter (e.g., permeability) field. Instead, we modify the coarse grid operator to include internal fine grid information and produce an upscaled solution (pressure and velocity) directly. The method seeks to overcome some of the more serious short-comings of traditional upscaling methods by making use of the mixed finite element method (a rigorous mathematical formulation amenable to error analysis) as well as the original domain boundary conditions. Because we never solve

the full fine grid problem, the method is a feasible upscaling idea when one is forced to run multiple flow simulations of a single field because of a geostatistical (and uncertain) description of the reservoir. We have illustrated the general idea in its simplest setting: i.e., the linear, single-phase pressure equation in 2D. Moreover, we assume the permeability matrix on the fine grid is diagonal but discontinuous. Nothing about the method prevents it from being applied to a more complicated set of equations.

The central idea is to solve the upscaled problem in two stages. First we solve n small δ-problems, with n being the number of coarse grid blocks. We have made use of a closure assumption requiring each of these δ-problems to have homogeneous Neumann boundary conditions. This assumption allows us to solve each of these n problems independently (ideal for a parallel implementation). We solve these problems only for the fine grid unknowns *internal* to each coarse grid block. The second step of the process involves constructing and solving a problem with unknowns defined only on the coarse grid. The linear operators in this upscaled problem are modified to include the fine grid information we obtain from step 1. We use fine scale quadrature and the original fine grid permeability field in both steps.

We performed upscaling experiments on three very different permeability fields, varying the size of the final coarse grid and the domain boundary conditions. We compare the new operator-based upscaling method to two traditional techniques — harmonic averaging and the pressure solver approach. The results indicate that the new method does a comparable job to the other methods in most situations and overcomes obstacles often encountered with more standard approaches. It gives qualitatively the correct solution when there is a high permeability streak diagonal to the direction of fluid flow and when the boundary conditions are not standard. For the third permeability field we also see that the method does a good job of modeling fluid trapped by shale barriers. The standard approaches tend to smear out the pressure rather than capturing local features of the flow field.

There are many directions for extending this work. Perhaps the most important is to attempt a rigorous error analysis of the upscaling method in the context of the MFEM to pinpoint when the method is most and least accurate. We could also extend the method numerically to a more sophisticated setting such as three dimensions, two-phase flow, a non-diagonal permeability tensor, and a nonlinear operator equation. However, what we have demonstrated in this paper is that the general idea of deriving an effective solution rather than an effective input parameter field holds promise for upscaling.

Acknowledgments. We are especially grateful to Mike Christie of British Petroleum for guiding us with his insight and interest in upscaling as well as for providing us with the pressure solver code and the permeability data for the last two examples. We thank Grant Robertson of British Petroleum, and Mary Wheeler and Clint Dawson of the University of Texas at Austin for their support of this project. The second author was supported by the National Science Foundation and British Petroleum under NSF-Industrial Postdoc Grant #DMS-9696-008.

Numerical Upscaling Experiments					
Expt. No./Case No./Permeability	Fine Grid	Upscaled Grid	BC	Pressure Error	Velocity Error
Expt. 1/Case 1/Diagonal	40x40	4x4	S		
Operator-Based				.06071	.96487
Harmonic Averaging				.06958	.96809
Pressure Solver				.12012	.96177
Expt. 2/Case 1/Case 6 slice	32x32	16x16	S		
Operator-Based				.02294	.09831
Harmonic Averaging				.00774	.05242
Pressure Solver				.00765	.05274
Expt. 2/Case 2/Case 6 slice	32x32	8x8	S		
Operator-Based				.01900	.17501
Harmonic Averaging				.02783	.13880
Pressure Solver				.02646	.13693
Expt. 2/Case 3/Case 6 slice	32x32	8x8	NS		
Operator-Based				.00788	.08431
Harmonic Averaging				.02528	.21441
Pressure Solver				.02701	.24115
Expt. 3/Case 1/Chevron	128x128	16x16	S		
Operator-Based				.23633	.72441
Harmonic Averaging				.05006	.16250
Pressure Solver				.04167	.14330
Expt. 3/Case 2/Chevron	128x128	16x16	NS		
Operator-Based				.11581	.46776
Harmonic Averaging				.22752	.43766
Pressure Solver				.25095	.48949
Expt. 3/Case 3/Chevron	128x128	8x8	NS		
Operator-Based				.13128	.35443
Harmonic Averaging				.31148	.48568
Pressure Solver				.33200	.51325

TABLE 4.1

Upscaling experiments. Note: under BC "S" stands for standard boundary conditions and "NS" stands for nonstandard boundary conditions (see Fig 5.1).

REFERENCES

[1] A. Bensoussan, J. L. Lion, and G. Papanicolaou, *Asymptotic Analysis for Periodic Structure*, North Holland, Amsterdam, 1978.

[2] A. Bourgeat, *Homogenized behavior of two-phase flows in naturally fractured reservoirs with uniform fractures distribution*, Comput. Methods Appl. Mech. Eng., 47 (1984), pp. 205–216.

[3] S. C. Brenner and L. R. Scott, *The mathematical theory of finite element methods*, Springer-Verlag, New York, 1994.

[4] M. Christie, *Upscaling for reservoir simulation*, J. Pet. Tech., 48 (1996), pp. 1004–1010.

[5] M. A. Christie, M. Mansfield, P. R. King, J. W. Barker, and I. D. Culverwell, *A renormalisation-based upscaling technique for WAG floods in heterogeneous reservoirs*, in Expanded Abstracts, San Antonio, TX., USA, 1995, Soc. Petroleum Eng. 29127, pp. 353–361.

[6] R. Dimitrakopoulos and A. J. Desbarats, *Geostatistical modeling of gridblock permeabilities for 3d reservoir simultors*, SPE Reservoir Engineering, 8 (1993), pp. 13–18.

[7] J. Douglas and J. Roberts, *Global estimates for mixed methods for second order elliptic equations*, Math. Comp., 44 (1985), pp. 39–52.

[8] L. Durlofsky, *Numerical calculation of equivalent grid block permeability tensors for heterogeneous porous media*, Water Resour. Res., 27 (1991), pp. 699–708.

[9] L. J. Durlofsky, R. A. Behrens, R. C. Jones, and A. Bernath, *Scale up of heterogeneous three dimensional reservoir descriptions*, in Expanded Abstracts, Dallas, TX., USA, 1996, Soc. Petroleum Eng. 30709, pp. 1–14.

[10] L. J. Durlofsky, R. C. Jones, and W. J. Milliken, *A new method for the scale up of displacement processes in heterogeneous reservoirs*, in 4th European Conference on the Mathematics of Oil Recovery: Expanded Abstracts, Roros, Norway, 1994.

[11] W. E, *Homogenization of scalar conservation laws with oscillatory forcing terms*, SIAM J. Appl. Math., 52 (1992), pp. 959–972.

[12] M. S. Espedal and O. Saevareid, *Upscaling of permeability based on wavelet representation*, in 4th European Conference on the Mathematics of Oil Recovery: Expanded Abstracts, Roros, Norway, 1994.

[13] T. Y. Hou and X. H. Wu, *A multiscale finite element method for elliptic problems in composite materials and porous media*, J. Comput. Phys., 134 (1997), pp. 169–189.

[14] J. Hyman, M. Shashkov, and S. Steinberg, *The numerical solution of diffusion problems in strongly heterogeneous non-isotropic materials*, J. Comput. Phys., 132 (1997), pp. 130–148.

[15] M. J. King, P. R. King, C. A. McGill, and J. K. Williams, *Effective properties for flow calculations*, Transport in Porous Media, 20 (1995), pp. 169–196.

[16] P. King and J. Williams, *Upscaling permeability: mathematics of renormalization*, in 4th European Conference on the Mathematics of Oil Recovery: Expanded Abstracts, Roros, Norway, 1994.

[17] P. R. King, A. H. Muggeridge, and W. G. Price, *Renormalization calculations of immiscible flow*, Transport in Porous Media, 12 (1993), pp. 237–260.

[18] S. Knapek, *Matrix-dependent multigrid-homogenization for diffusion problems*, In Situ, to appear (1997).

[19] T. C. Oppe, W. D. Joubert, and D. R. Kincaid, *NSPCG user's guide, version 1.0*, Technical Report 216, Center for Numerical Analysis, University of Texas at Austin, 1988.

[20] R. A. Raviart and J. M. Thomas, *Mathematical Aspects of the Finite Element Method, Lecture Notes in Math. 606*, Springer-Verlag, New York, 1977, ch. A mixed finite element method for 2nd order elliptic problems, pp. 292–315.

[21] T. F. Russell and M. F. Wheeler, *Finite element and finite difference methods for continuous flows in porous media*, in The Mathematics of Reservoir Simulation, Frontiers in Applied Math 1, R. E. Ewing, ed., Society for Industrial and Applied Mathematics, Philadelphia, 1983, pp. 35–106.

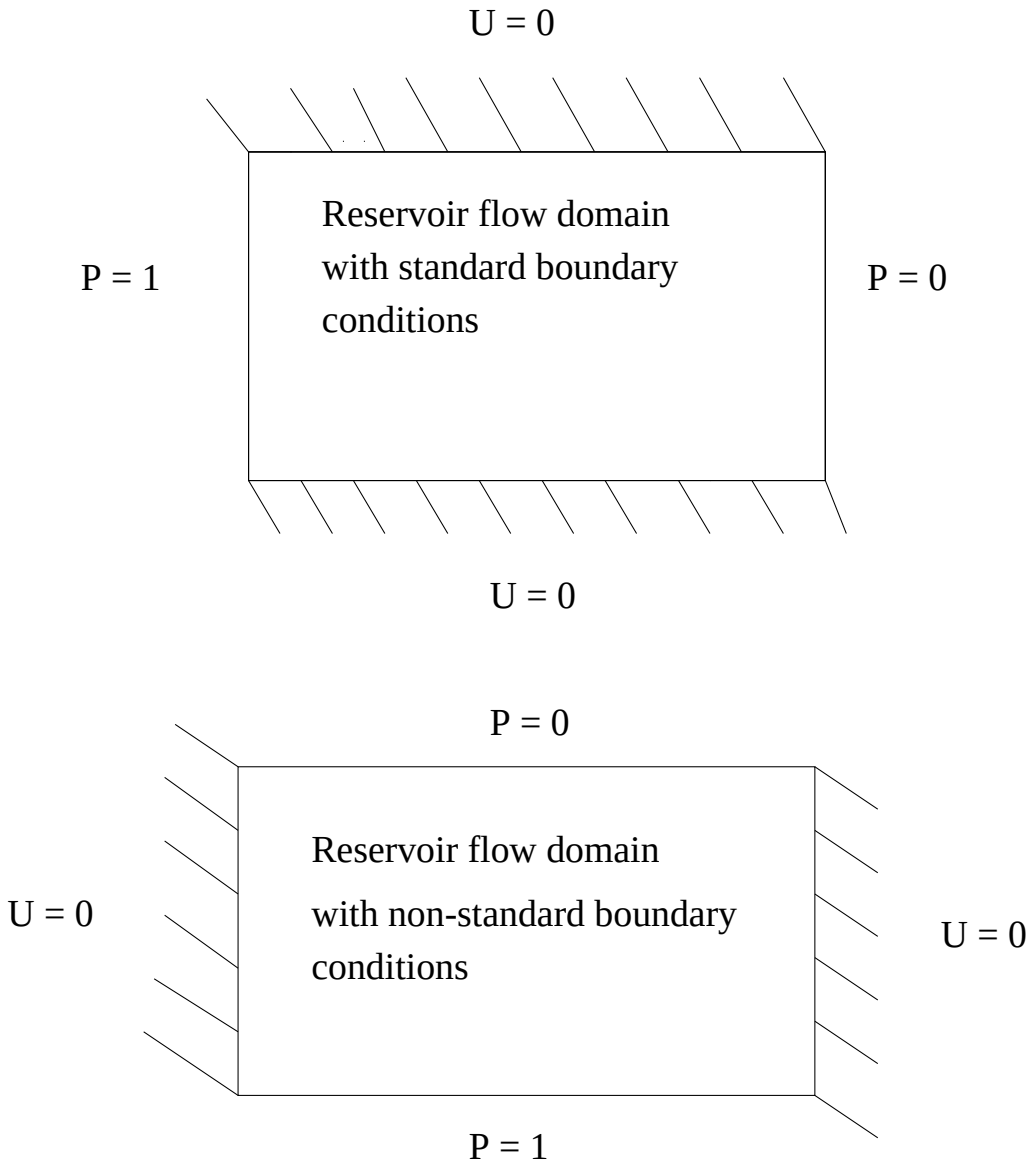

FIG. 5.1. *The two sets of global domain boundary conditions used in the numerical simulations.*

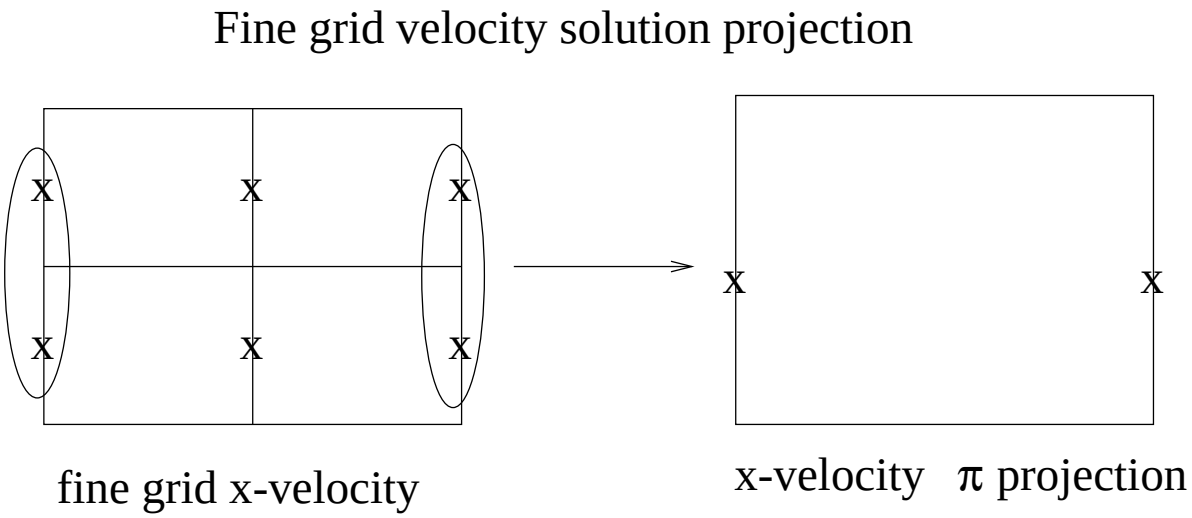

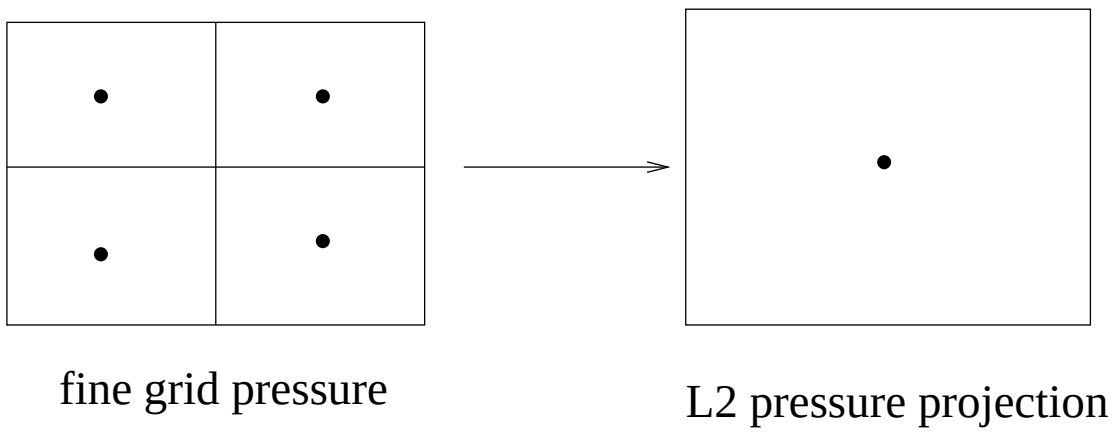

FIG. 5.2. *A schematic showing calculation of the L^2 fine grid pressure projection and the π fine grid velocity projection onto a single coarse grid block.*

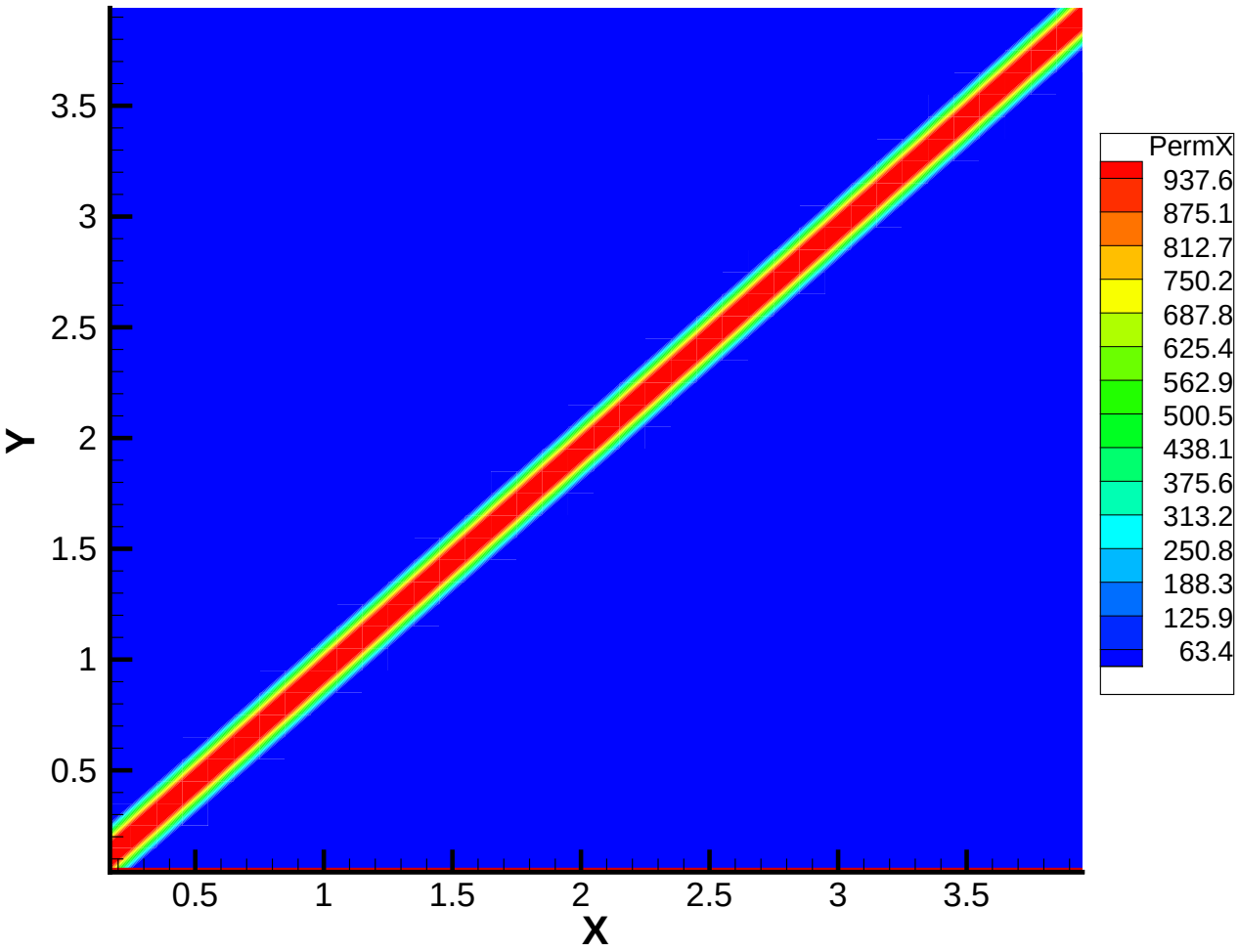

FIG. 5.3. *Example 1: the fine grid (40x40) permeability field.*

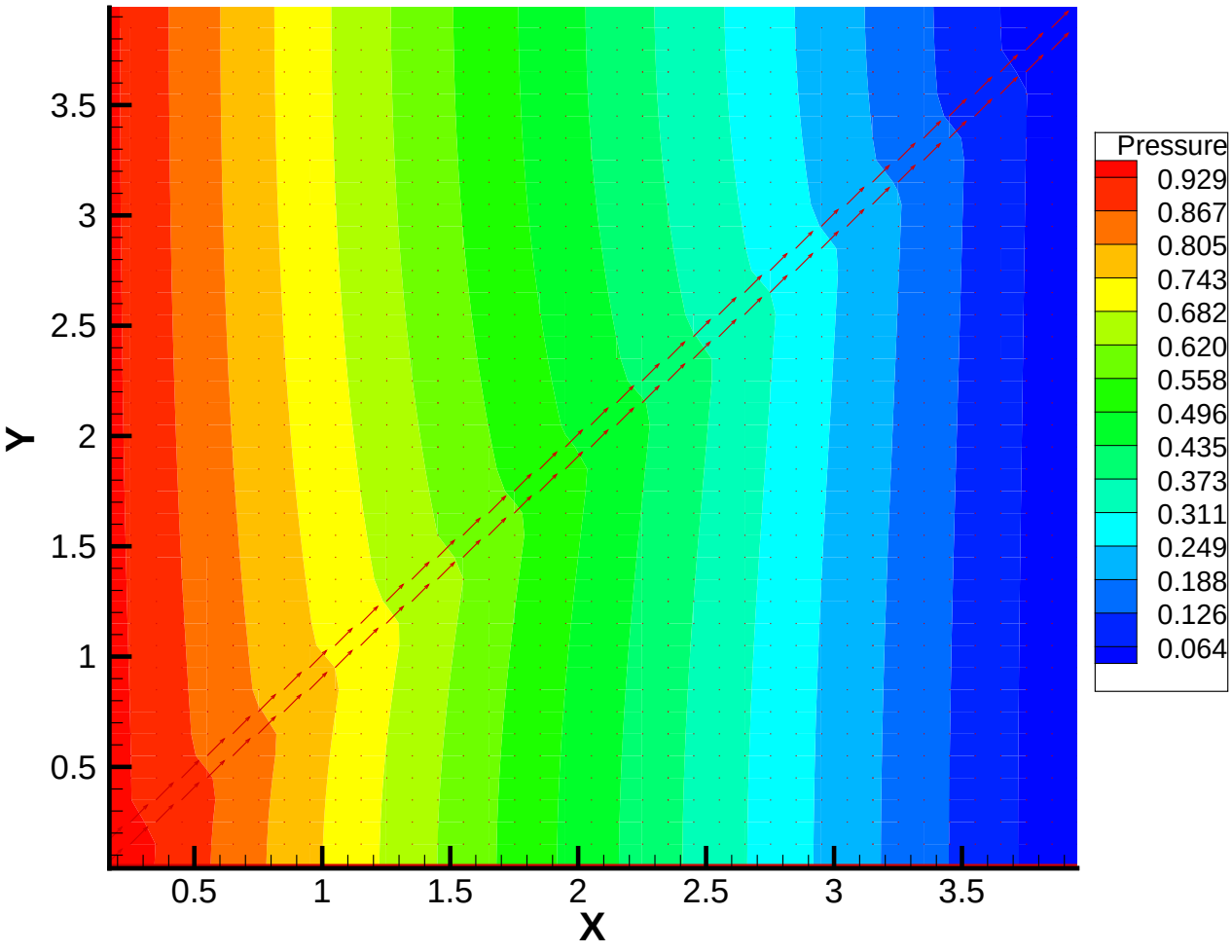

FIG. 5.4. *Example 1: the full fine grid (40x40) solution corresponding to the permeability field shown in Figure 5.3. Pressure is displayed as color contours. Vectors indicate fluid velocity. The boundary conditions are standard (see Figure 5.1).*

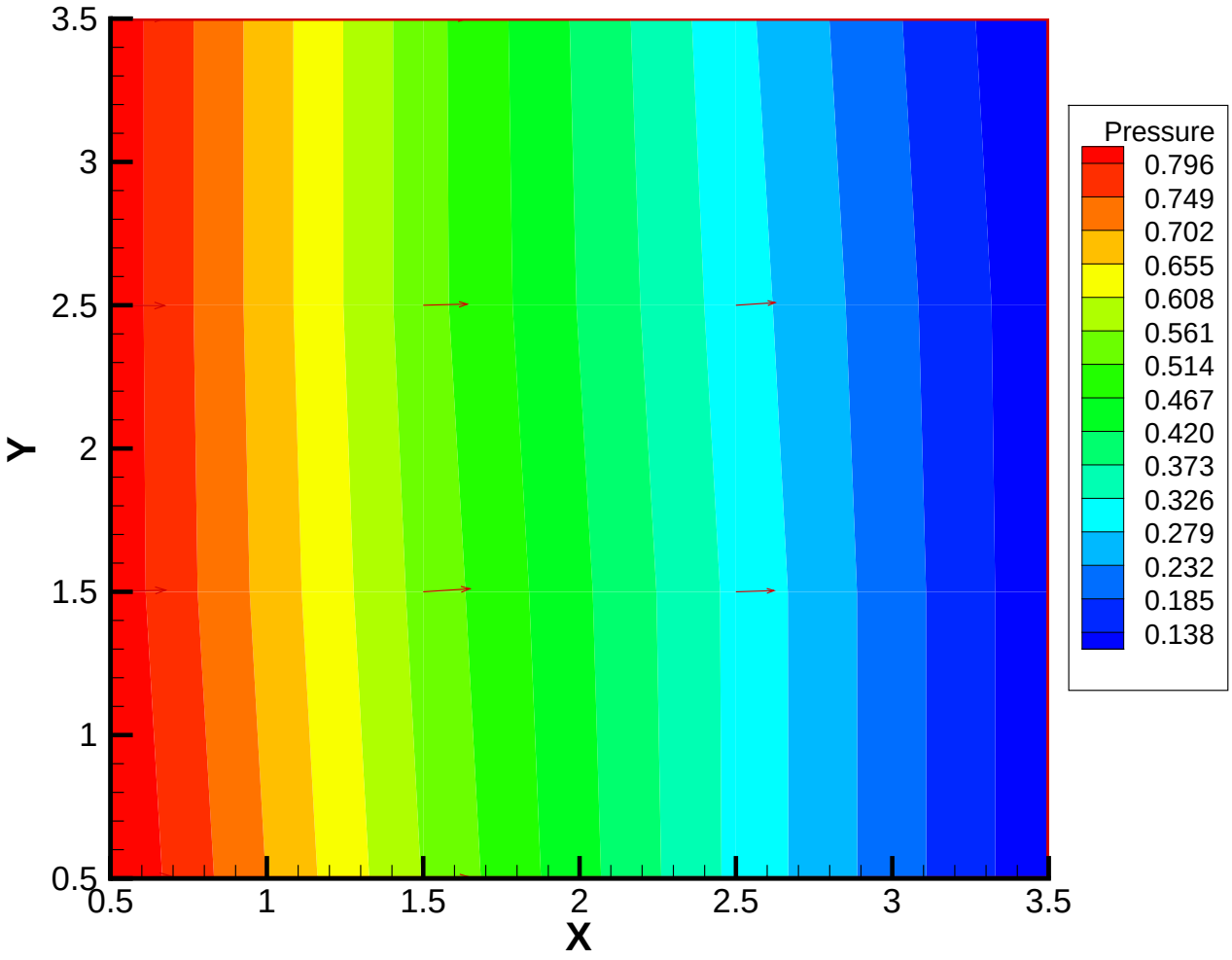

FIG. 5.5. *Example 1: the upscaled solution from a harmonic-average effective permeability field. The coarse grid is size 4x4.*

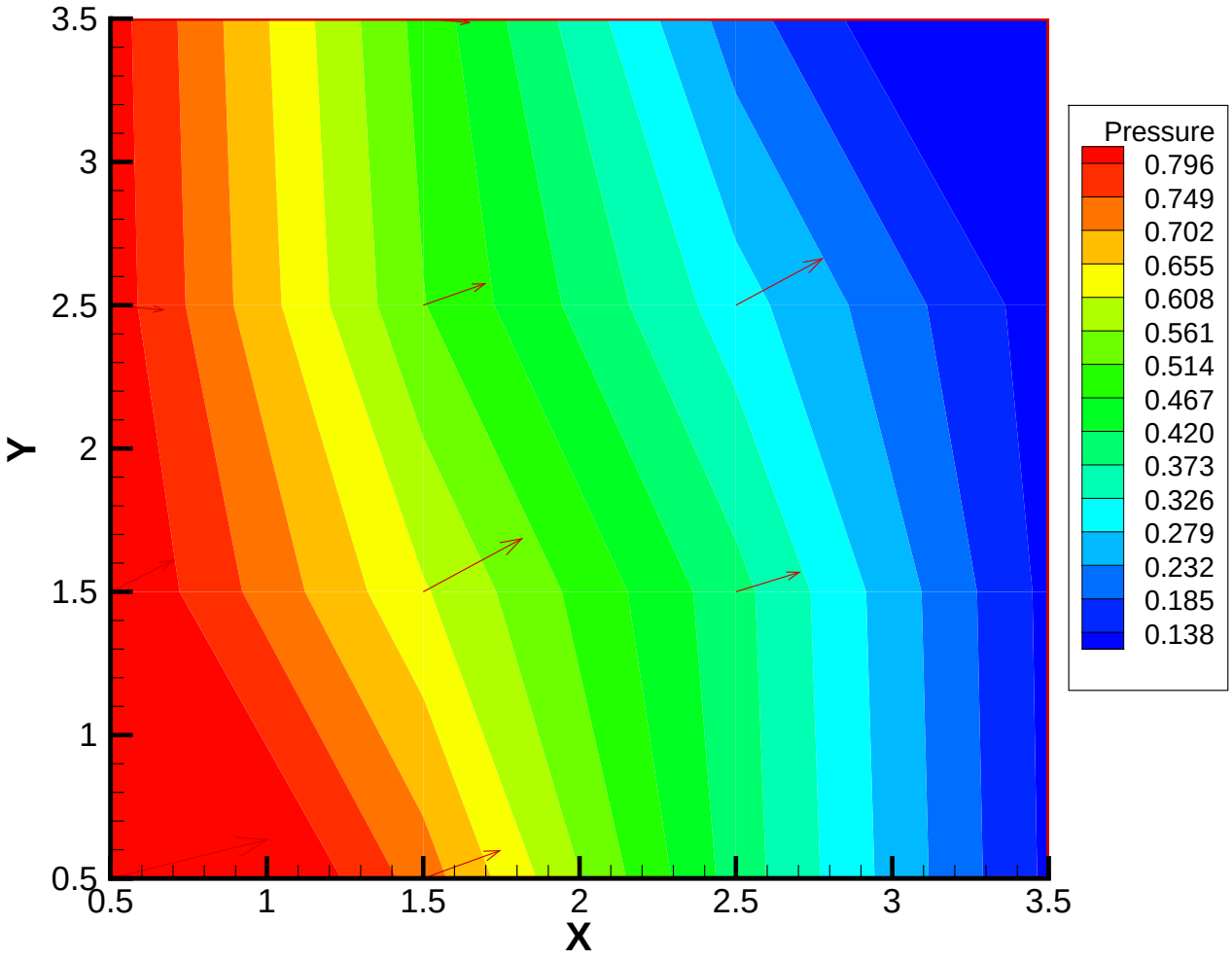

FIG. 5.6. *Example 1: the upscaled solution from a pressure-solver effective permeability field. The coarse grid is size 4x4.*

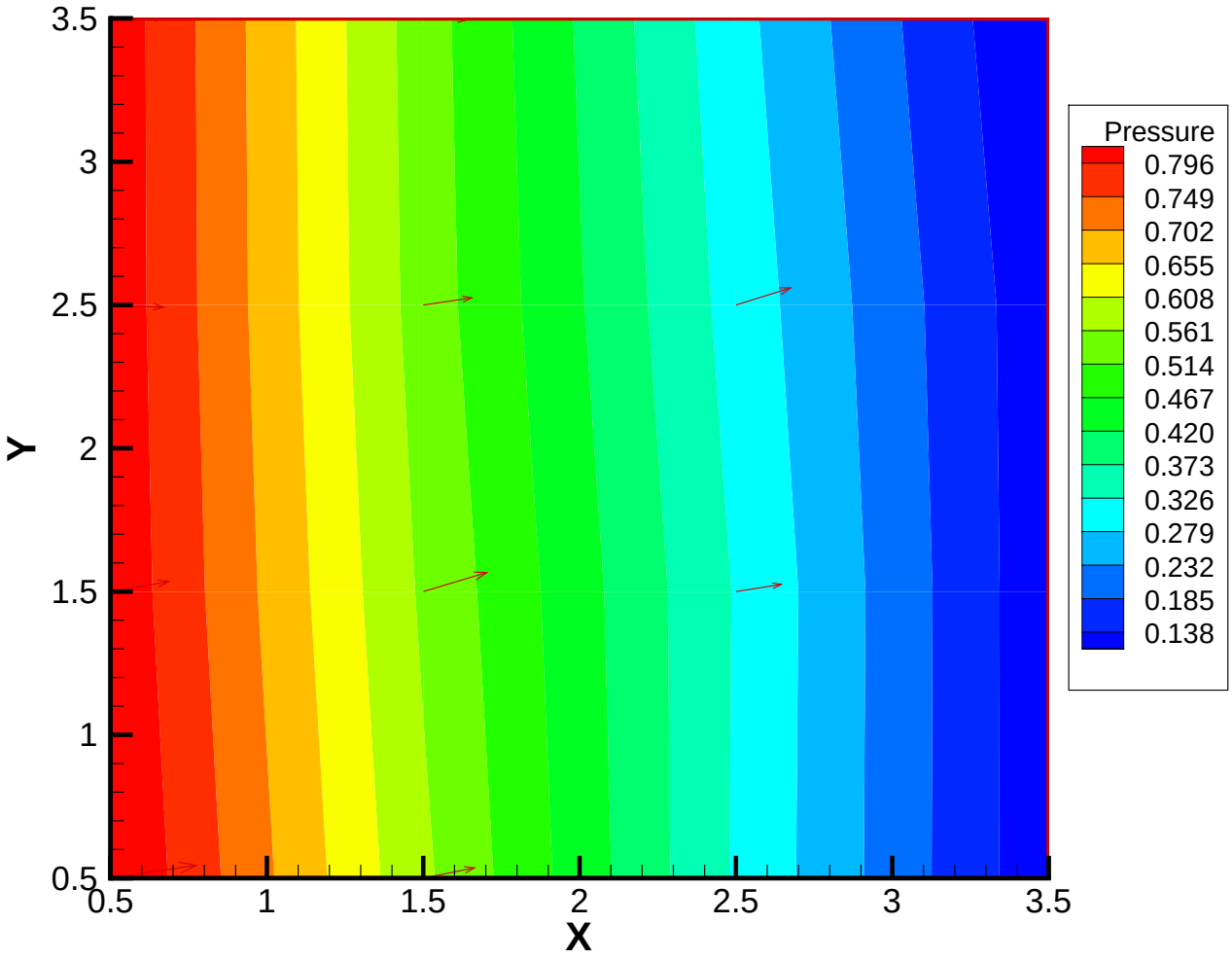

FIG. 5.7. *Example 1: the operator-based upscaled solution on a coarse grid of size 4x4.*

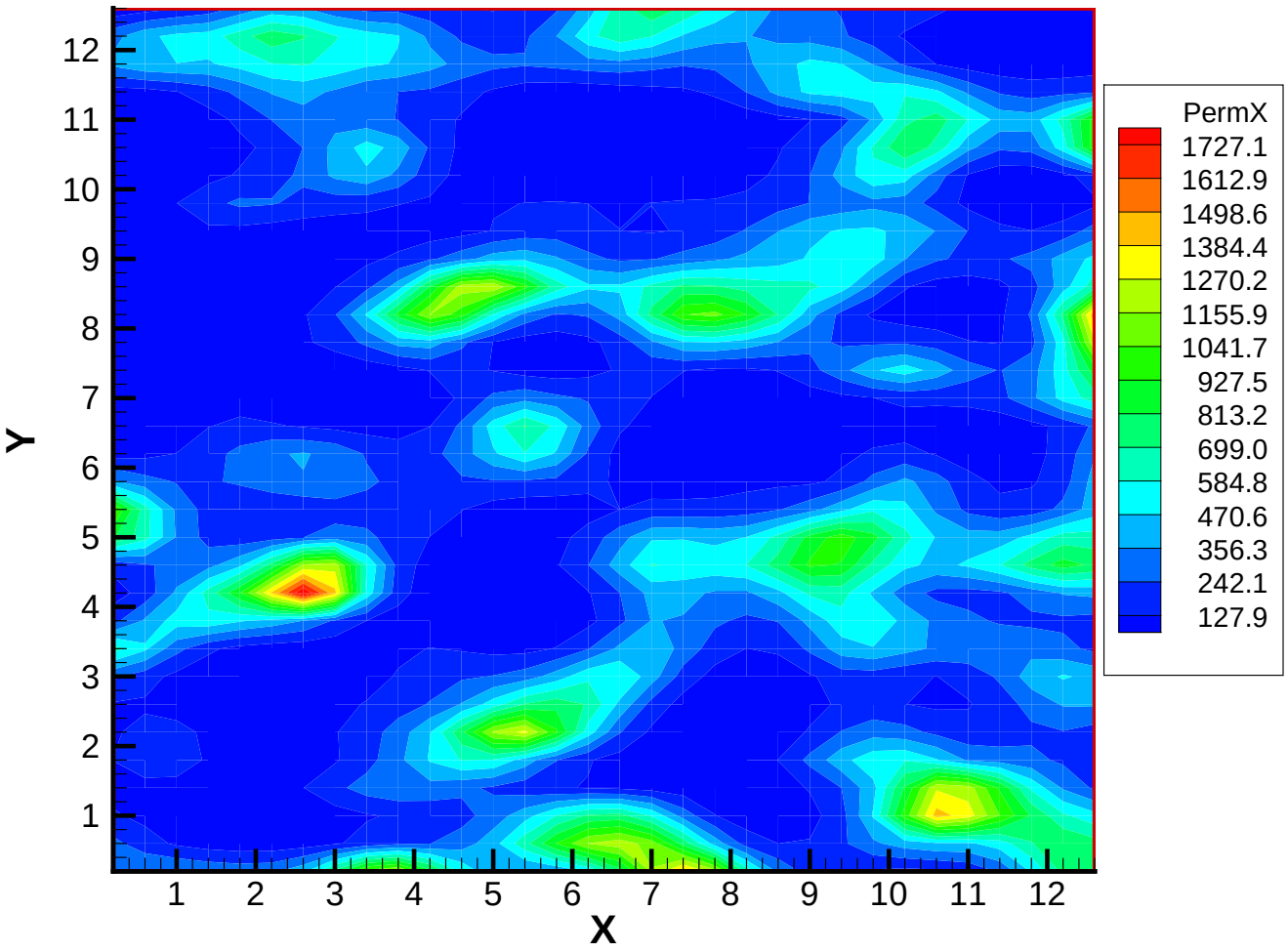

FIG. 5.8. *Example 2: the fine grid (32x32) permeability field (a 2D slice of the 3D "Case 6" permeability cube).*

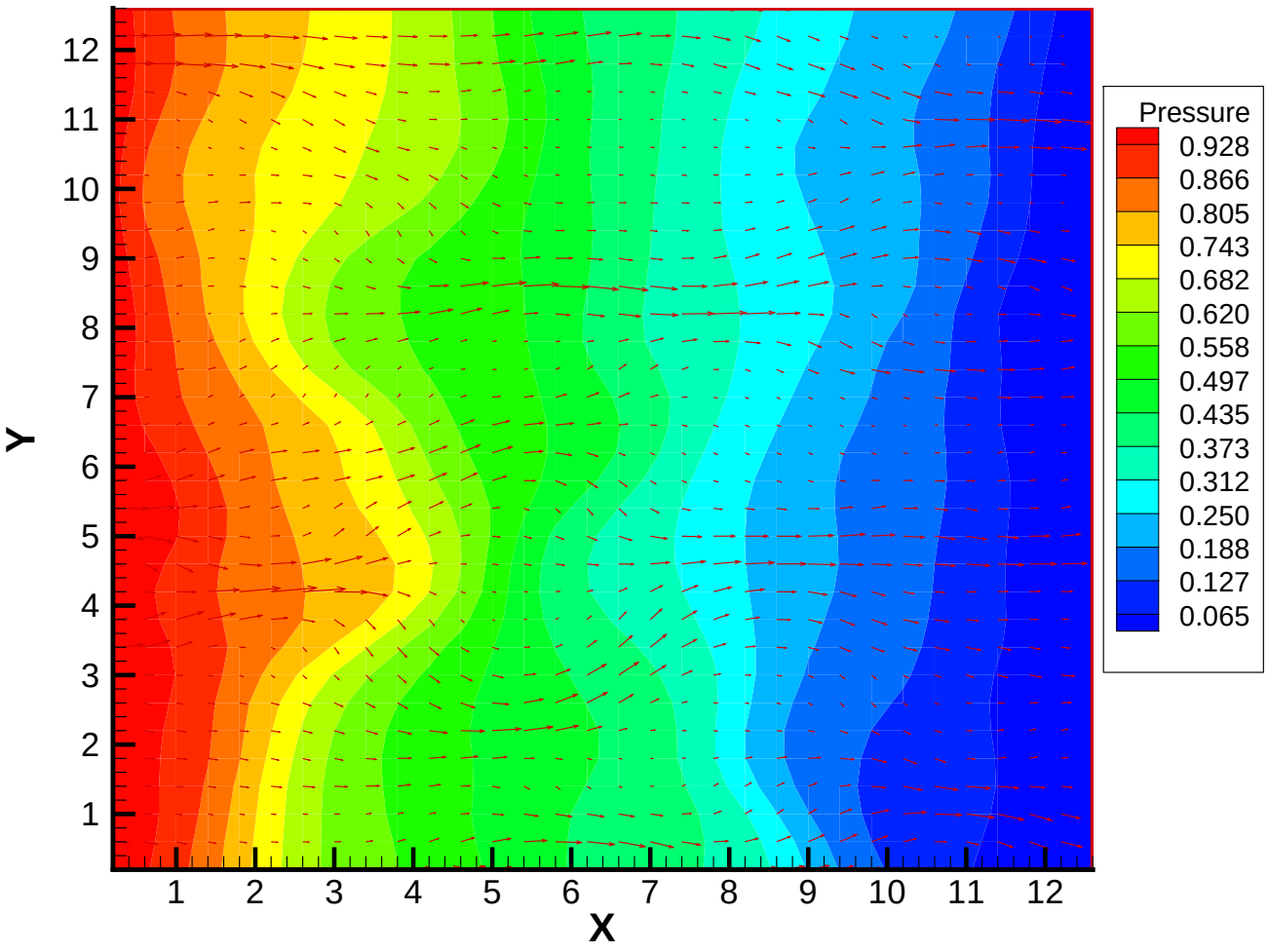

FIG. 5.9. *Example 2: the full fine grid (32x32) solution corresponding to the permeability field shown in Figure 5.8. The boundary conditions are standard (see Figure 5.1).*

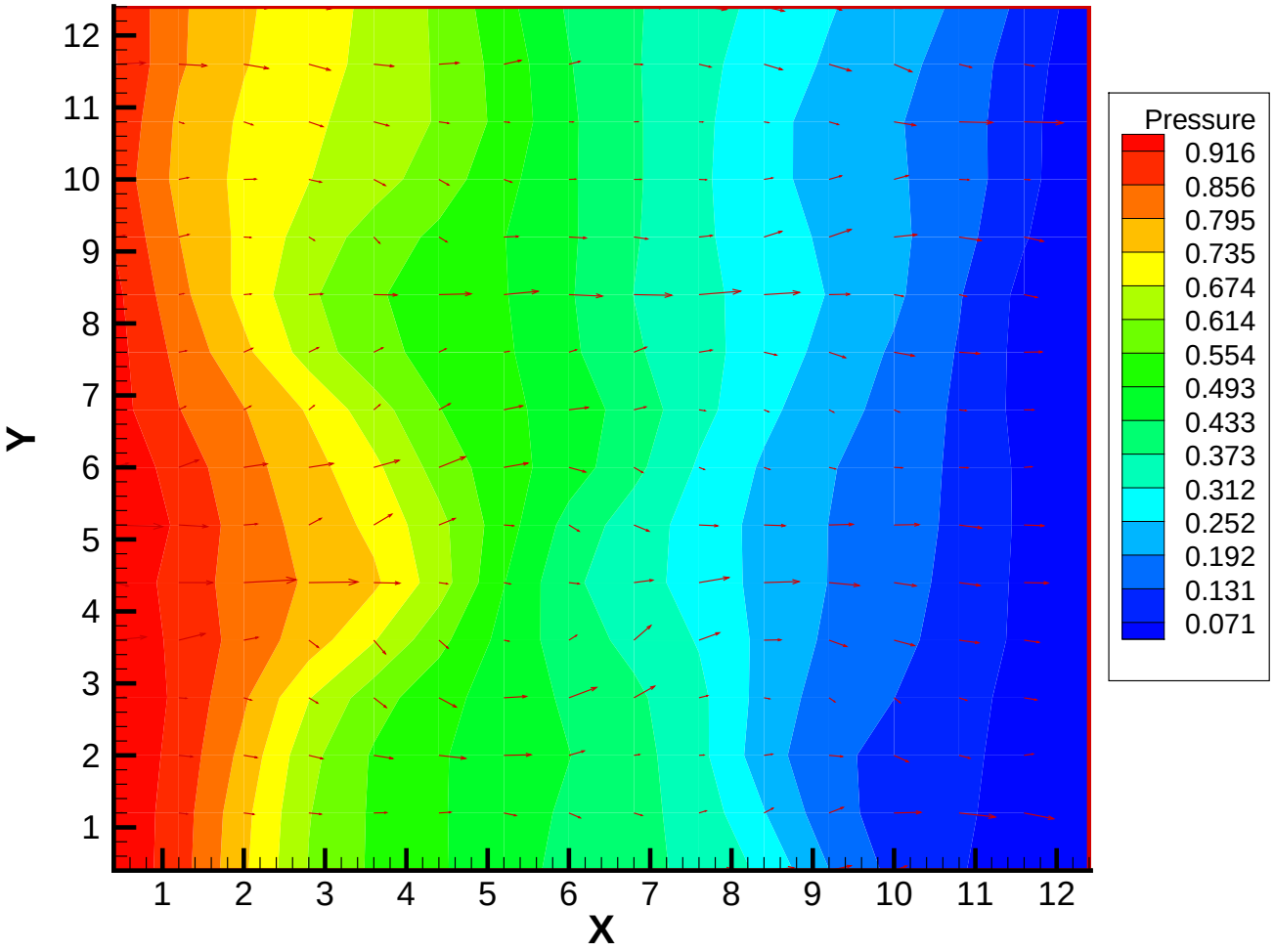

FIG. 5.10. *Example 2, Subcase 1: the operator-based upscaled solution on a coarse grid of size 16x16.*

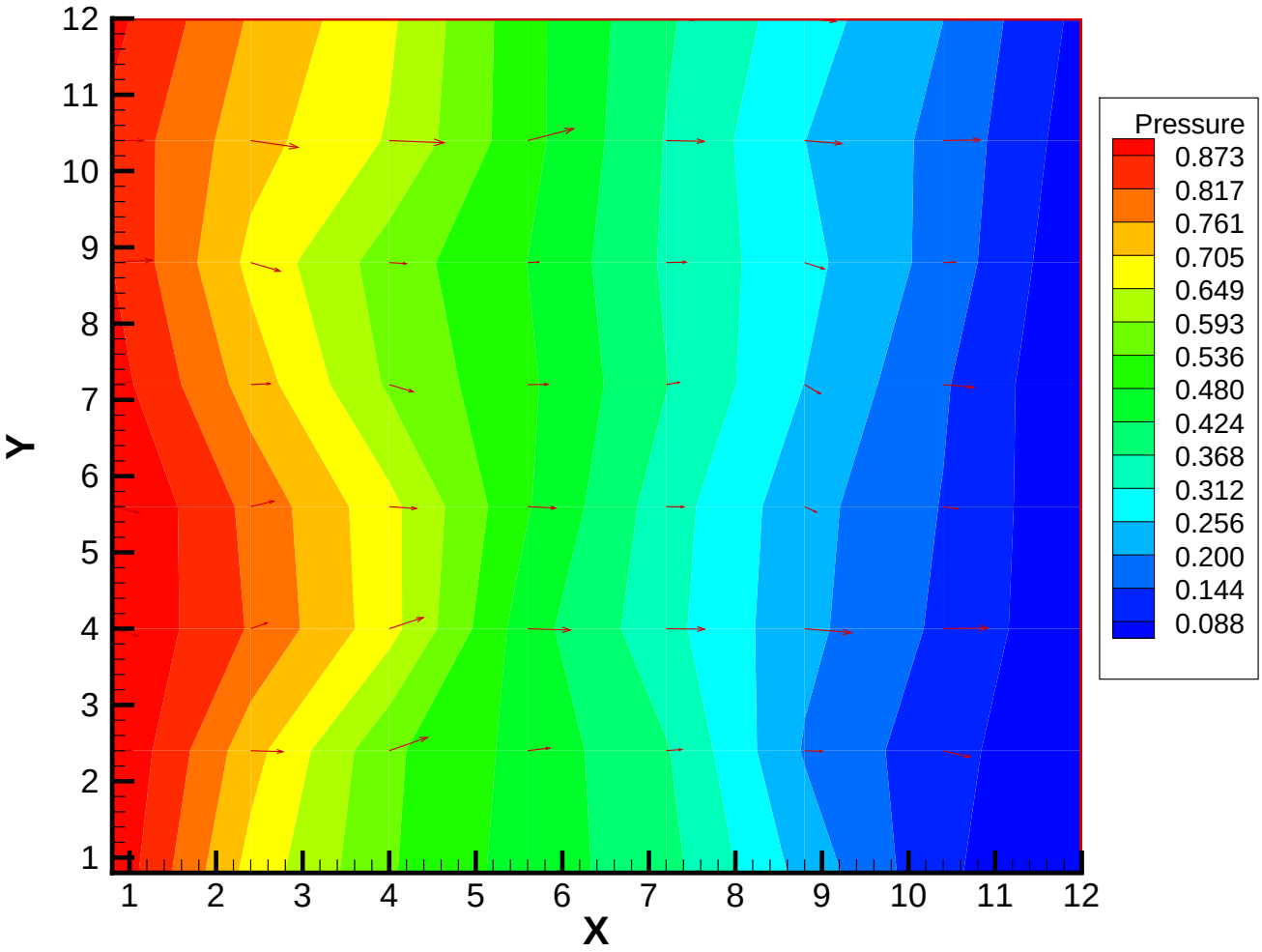

FIG. 5.11. *Example 2, Subcase 2: the projection of the full fine grid solution seen in Figure 5.9 onto an 8x8 coarse grid.*

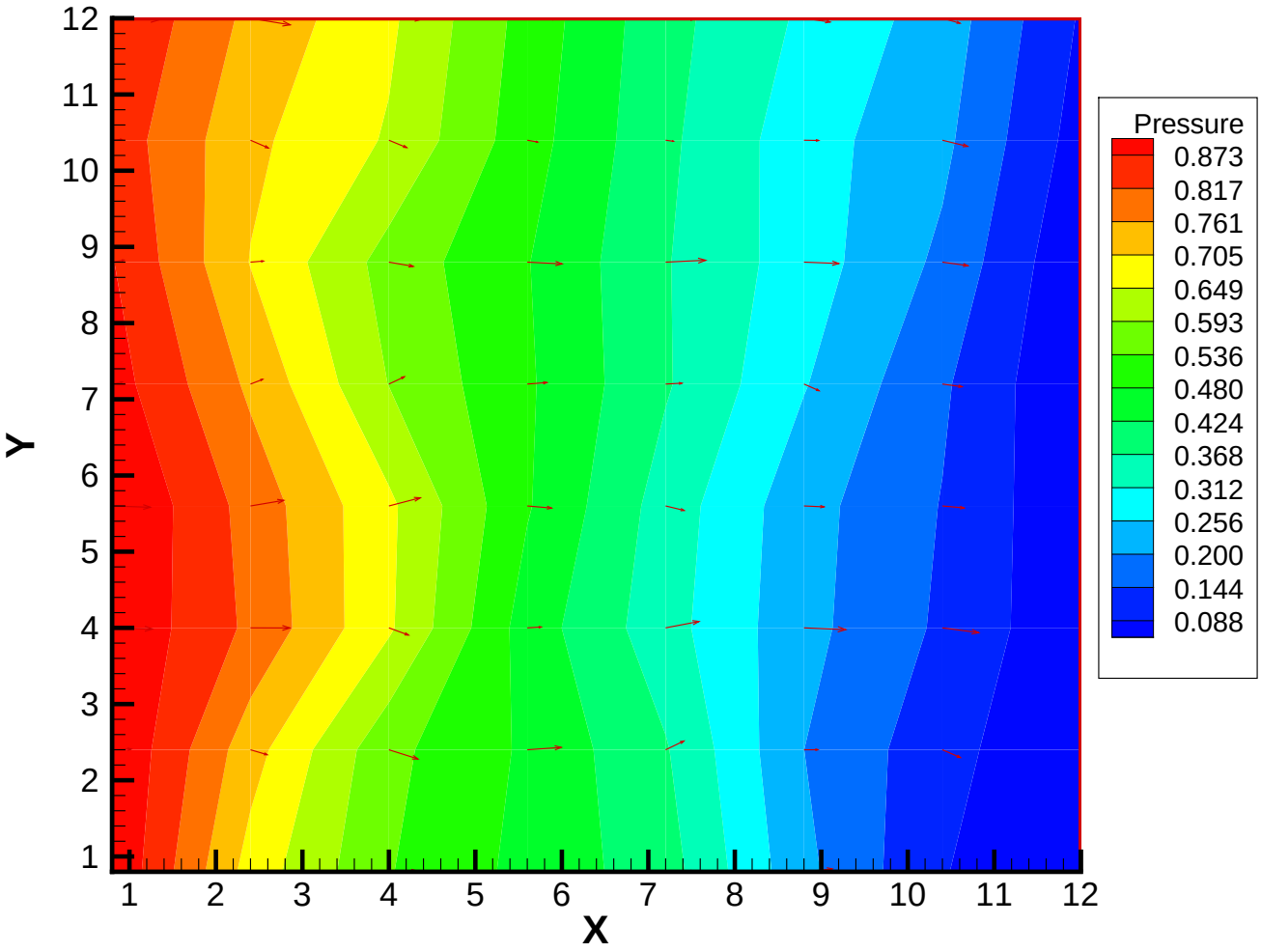

FIG. 5.12. *Example 2, Subcase 2: the operator-based upscaled solution on a coarse grid of size 8x8.*

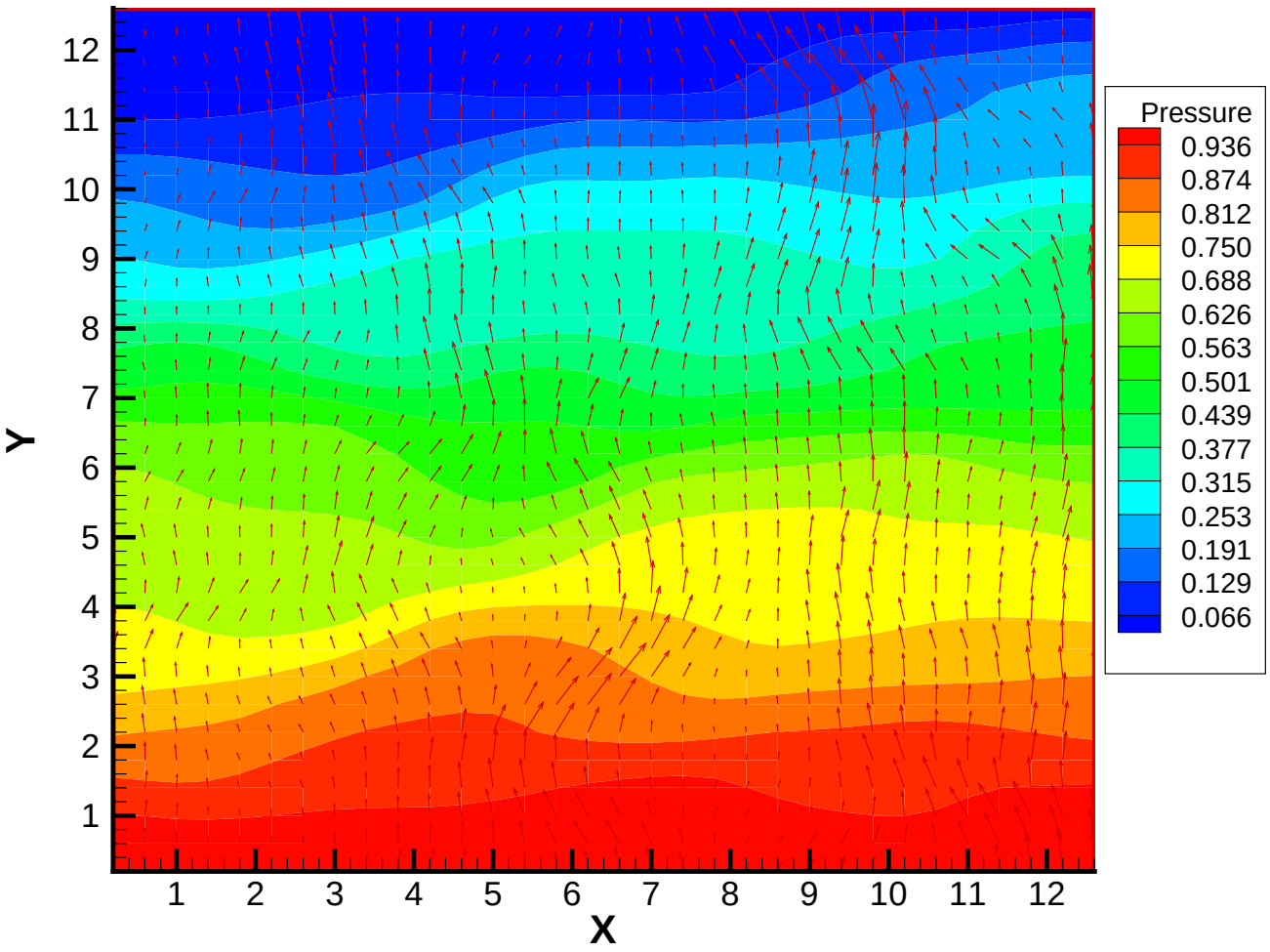

FIG. 5.13. *Example 2, Subcase 3: the full fine grid (32x32) solution corresponding to the permeability field shown in Figure 5.8. The boundary conditions are* non-standard *(see Figure 5.1).*

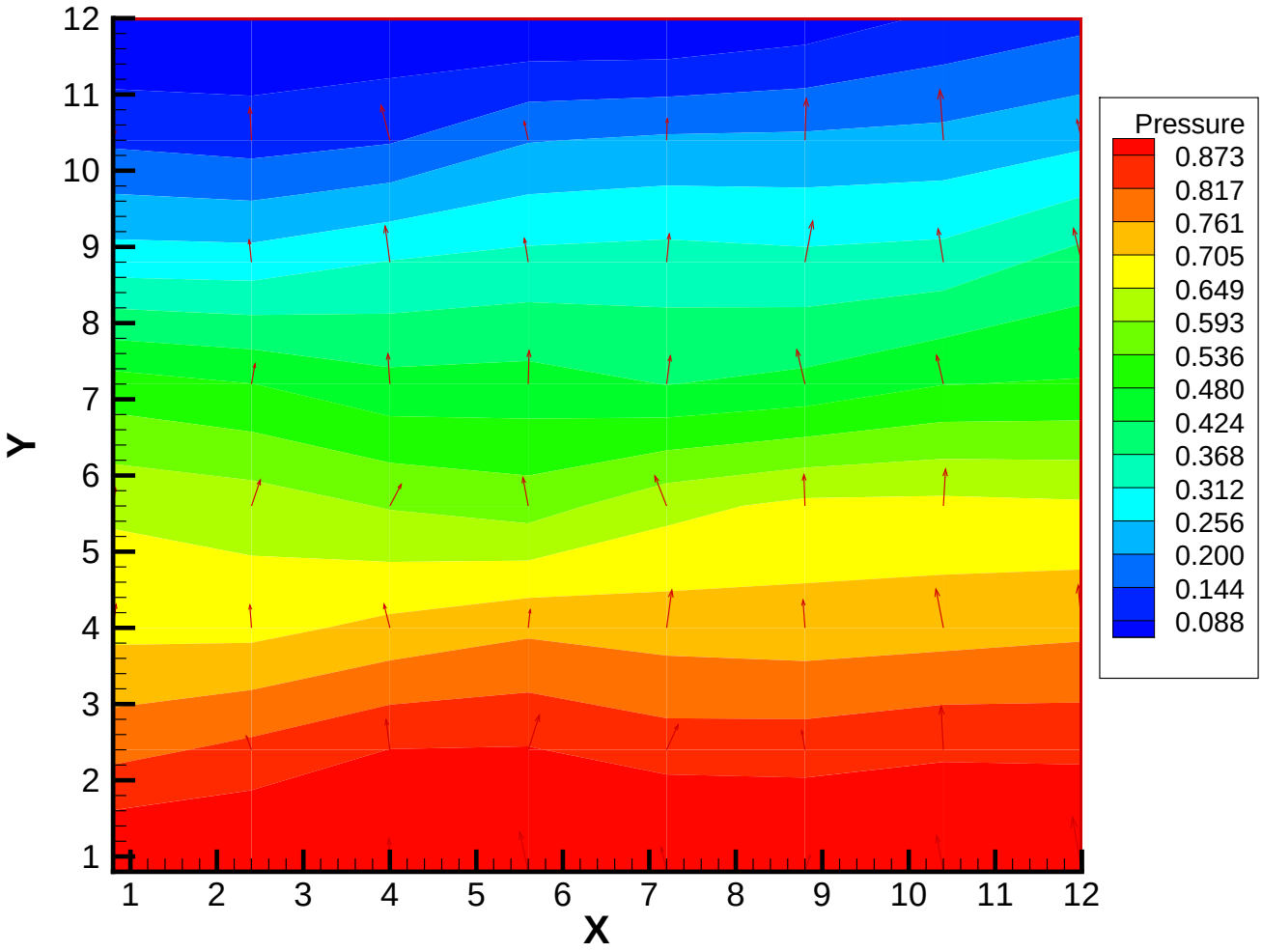

FIG. 5.14. *Example 2, Subcase 3: the operator-based upscaled solution on a coarse grid of size 8x8.*

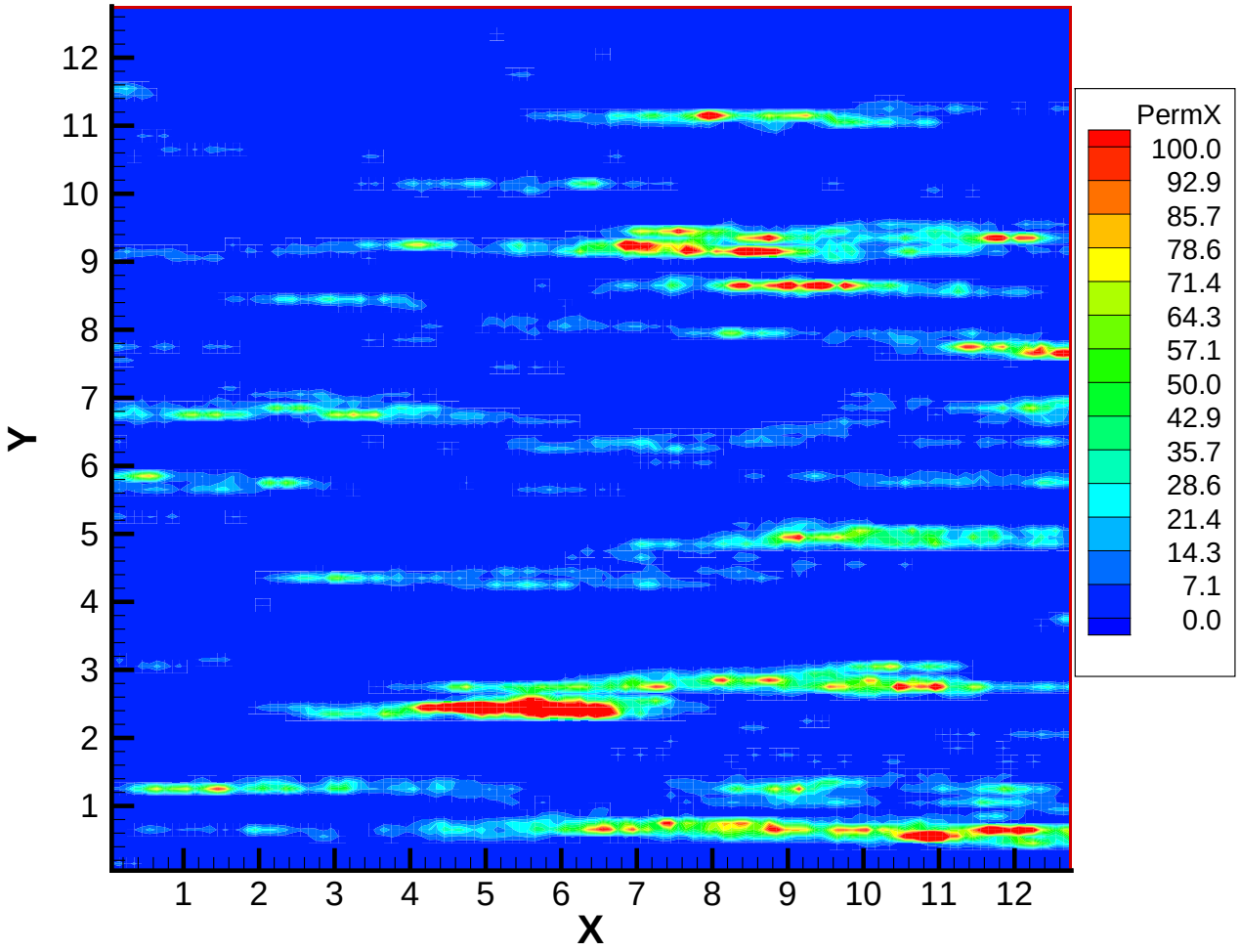

FIG. 5.15. *Example 3: the fine grid (128x128) permeability field.*

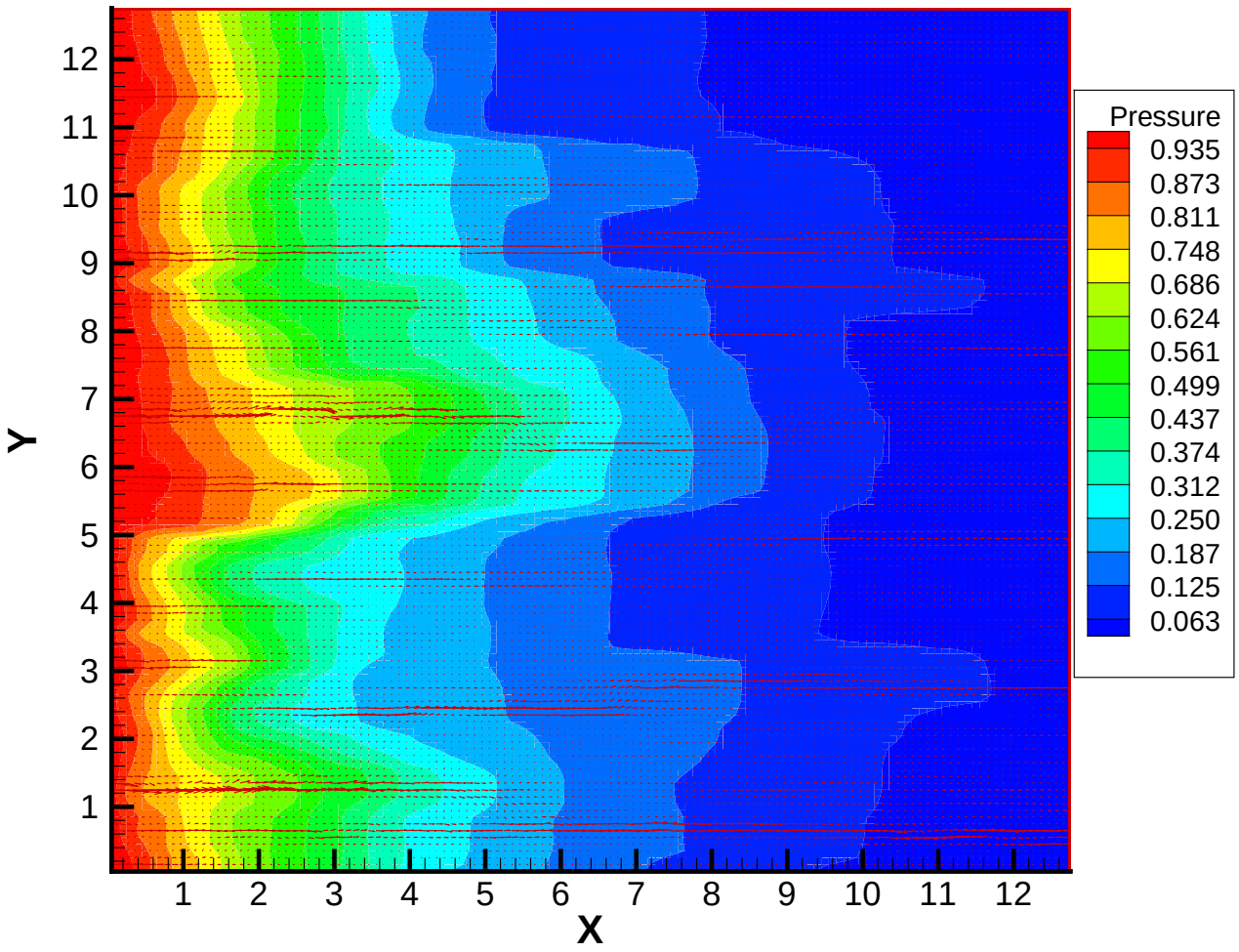

FIG. 5.16. *Example 3: the full fine grid (128x128) solution corresponding to the permeability field shown in Figure 5.15. The boundary conditions are standard (see Figure 5.1).*

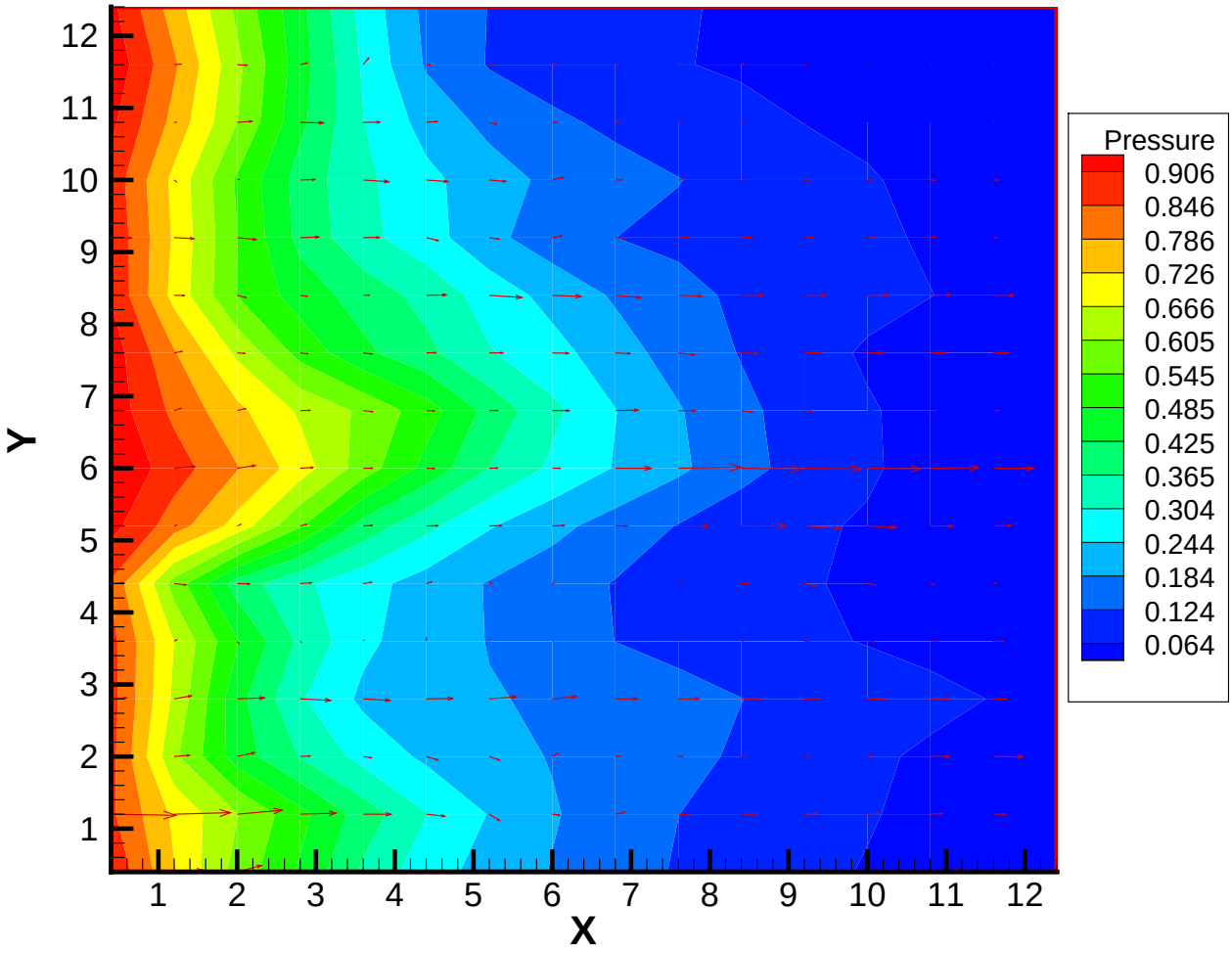

FIG. 5.17. *Example 3, Subcase 1: the projection of the full fine grid solution seen in Figure 5.16 onto a 16x16 coarse grid.*

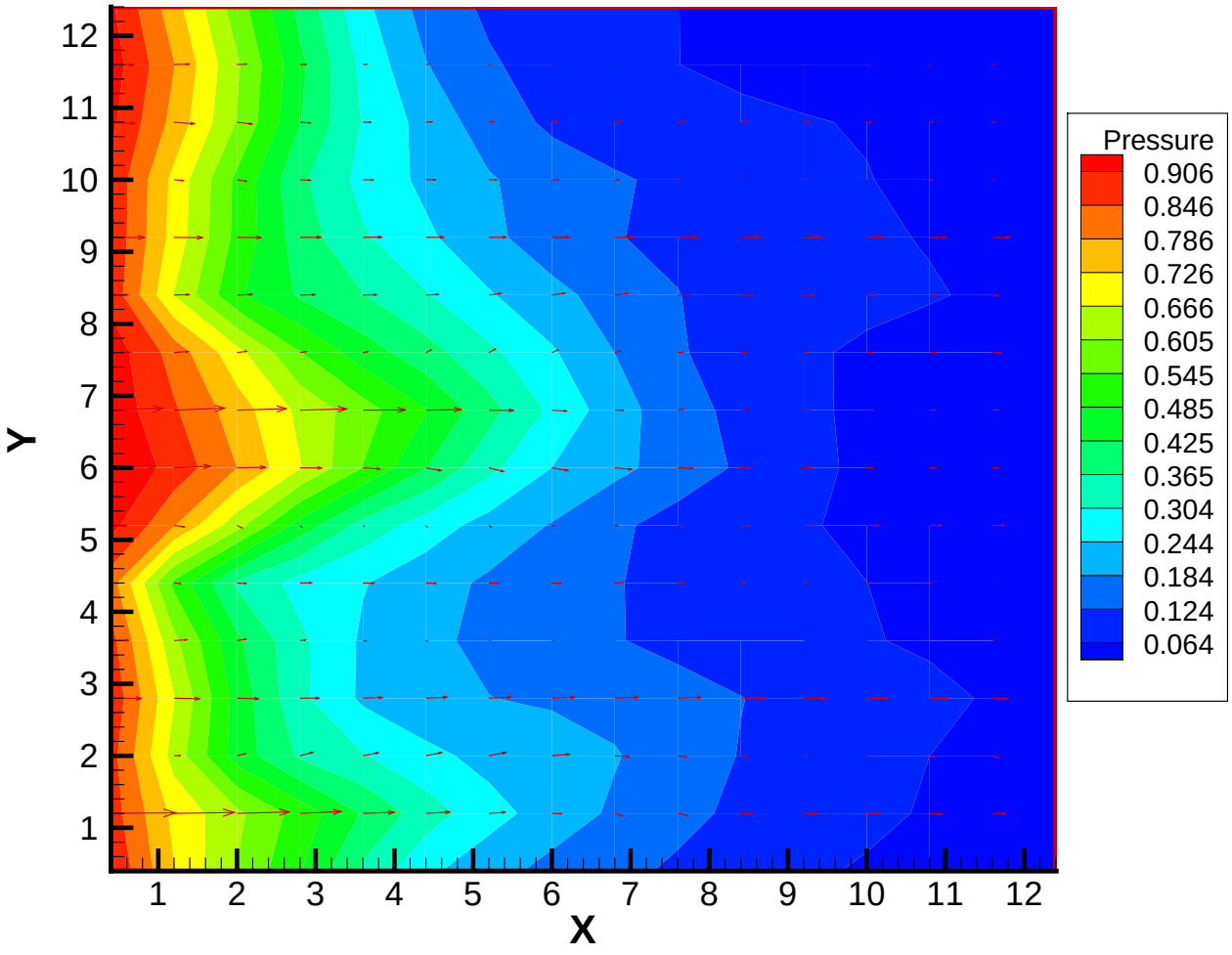

FIG. 5.18. *Example 3, Subcase 1: the upscaled solution from a harmonic-average effective permeability field. The coarse grid is size 16x16.*

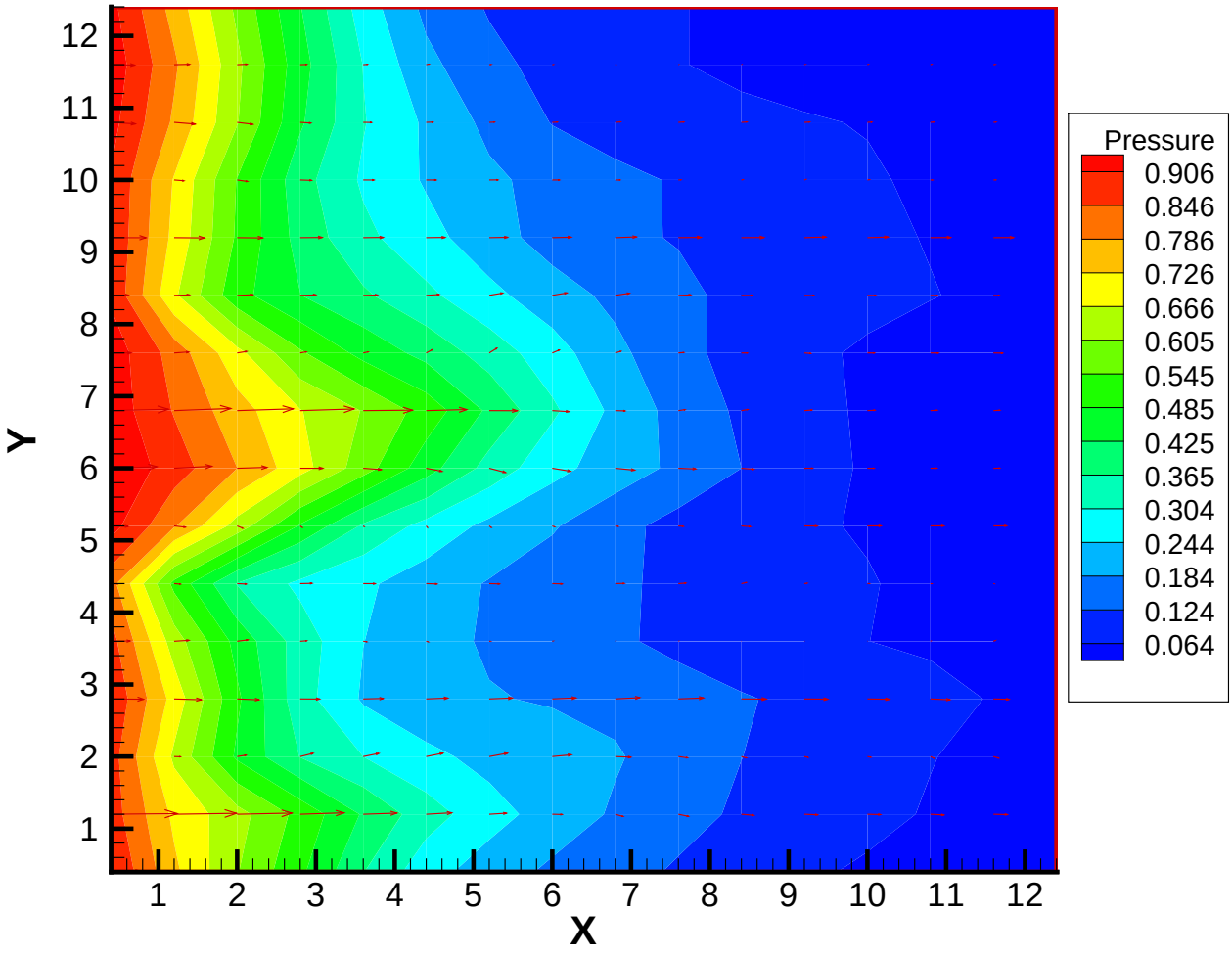

FIG. 5.19. *Example 3, Subcase 1: the upscaled solution from a pressure-solver effective permeability field. The coarse grid is size 16x16.*

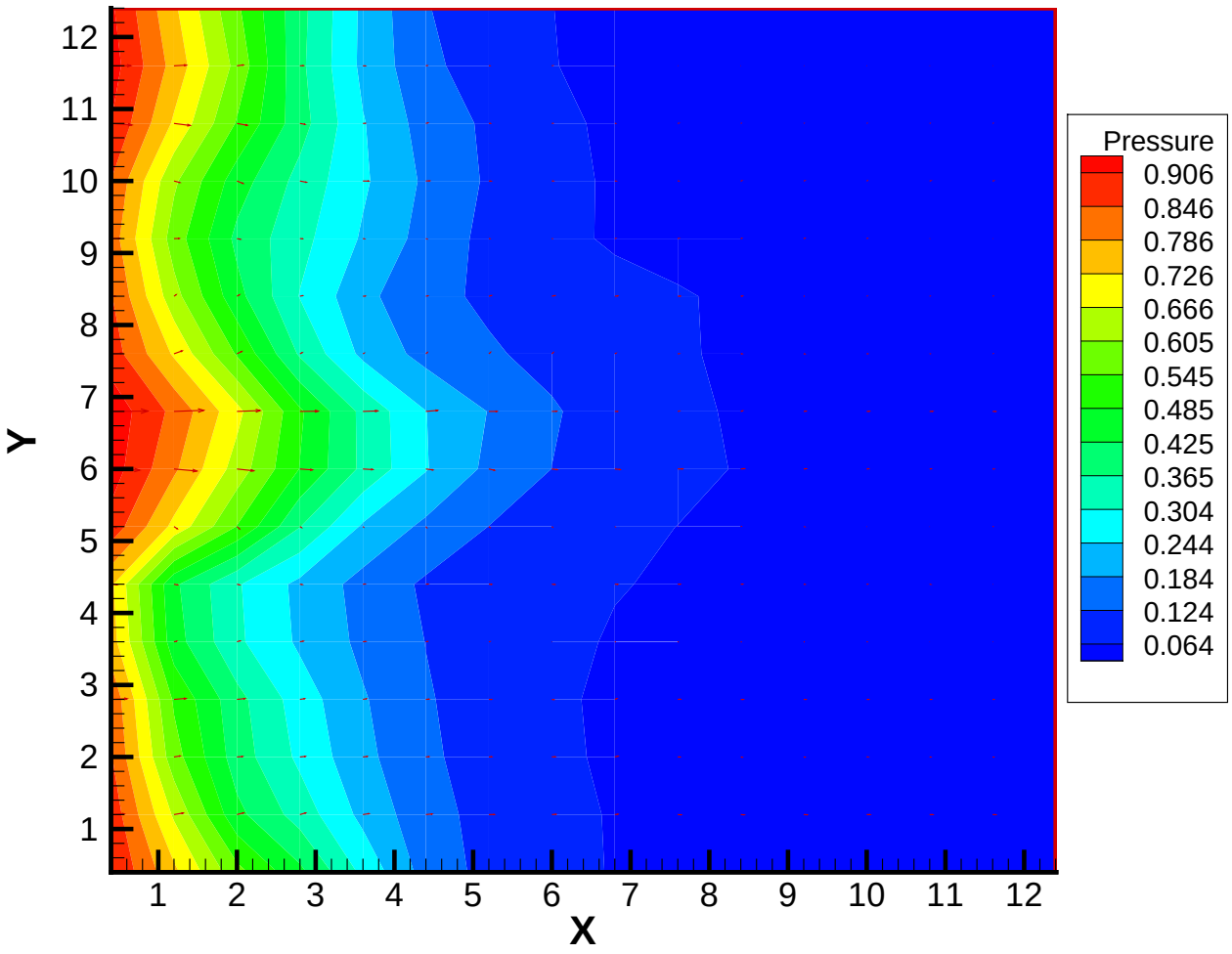

FIG. 5.20. *Example 3, Subcase 1: the operator-based upscaled solution on a coarse grid of size 16x16.*

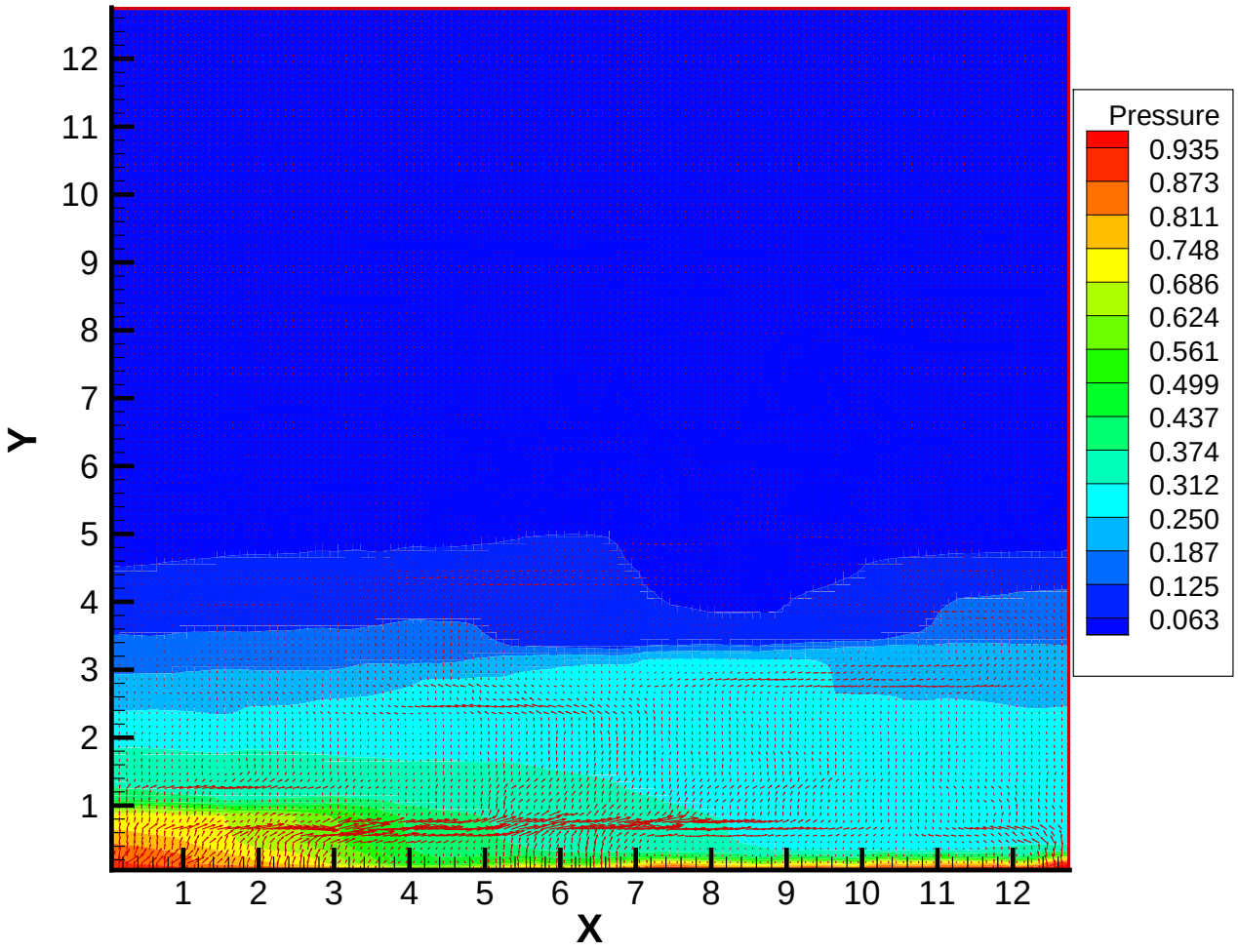

FIG. 5.21. *Example 3, Subcase 2: the full fine grid (128x128) solution corresponding to the permeability field shown in Figure 5.15. The boundary conditions are non-standard (see Figure 5.1).*

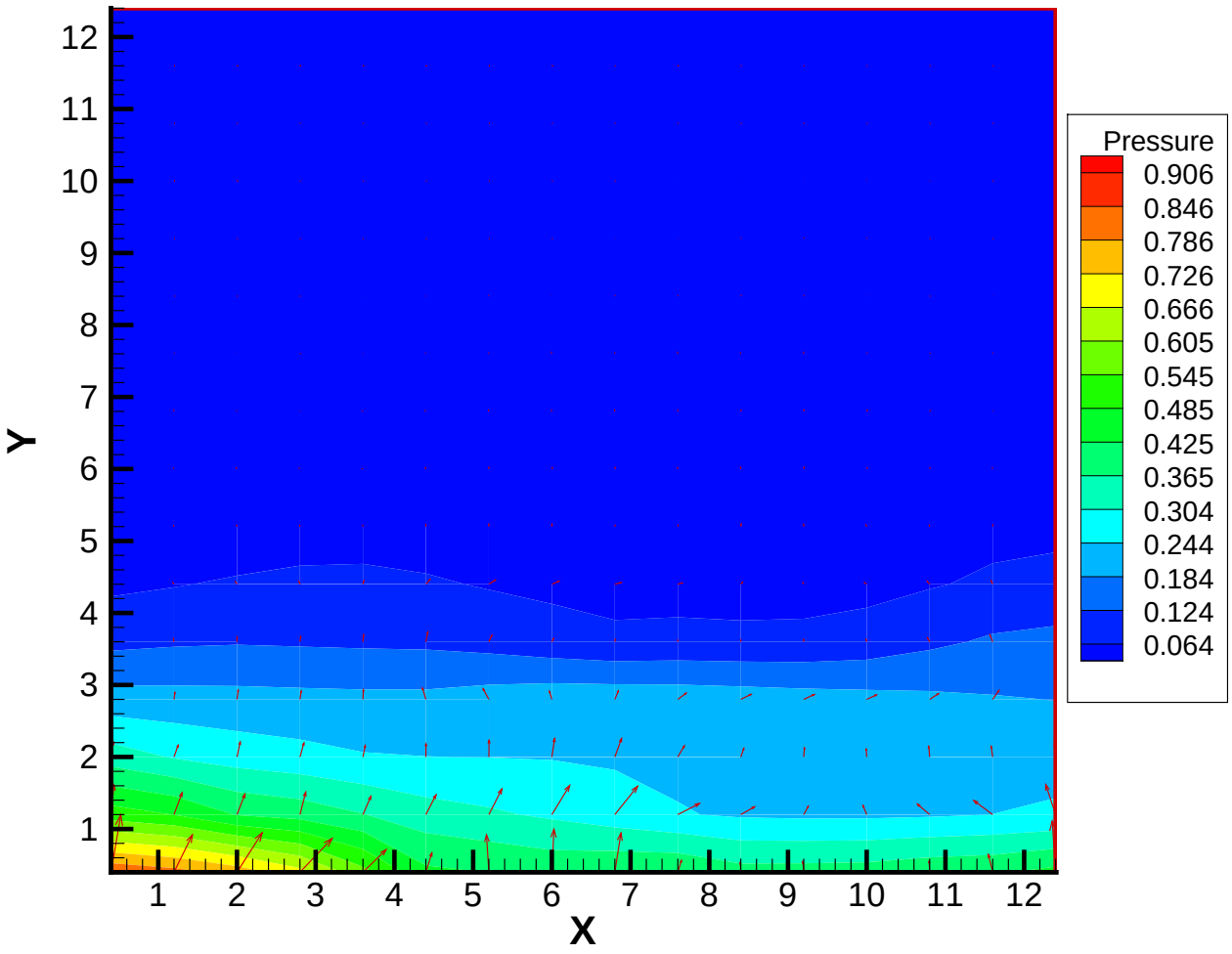

FIG. 5.22. *Example 3, Subcase 2: the operator-based upscaled solution on a coarse grid of size 16x16.*

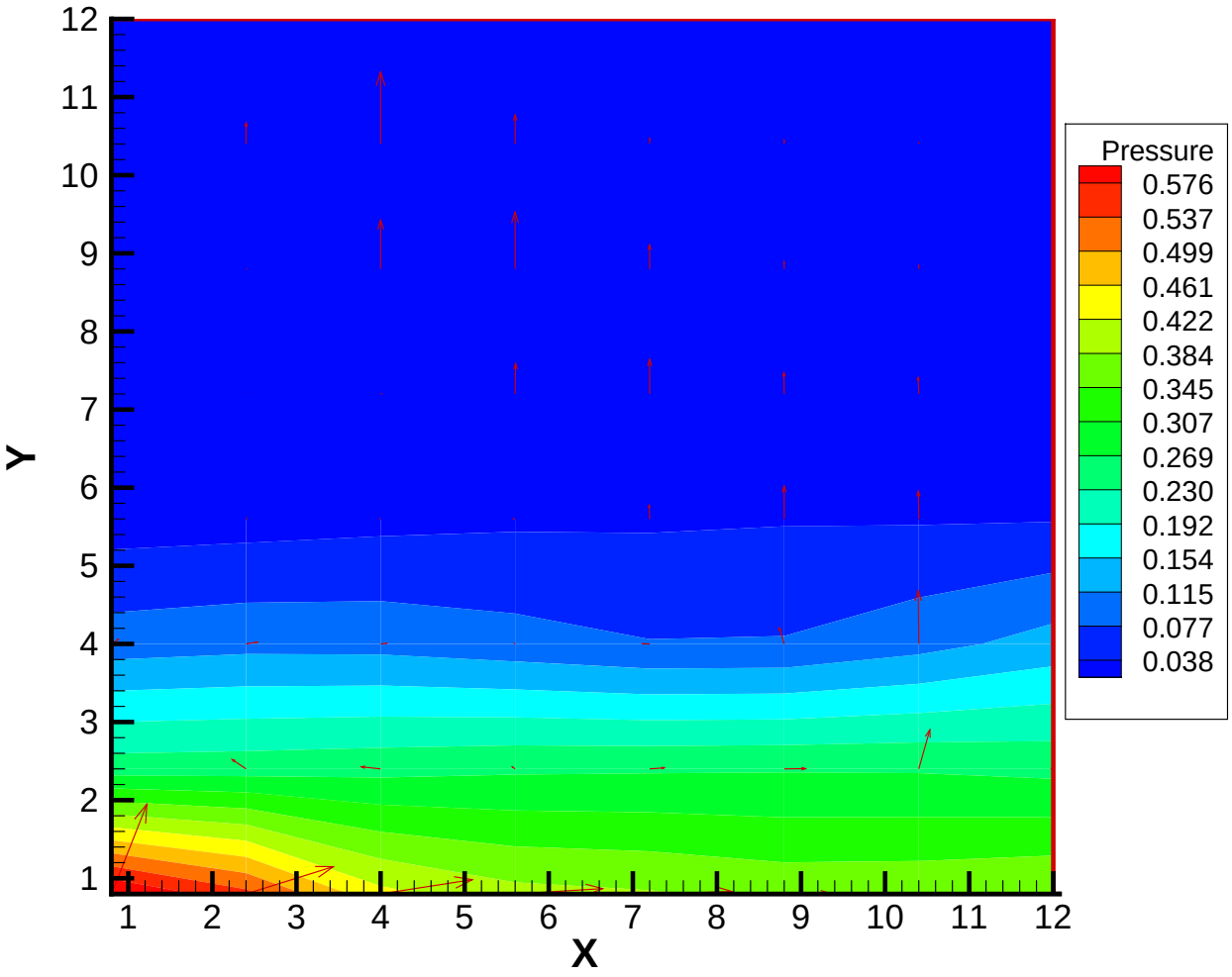

FIG. 5.23. *Example 3, Subcase 3: the projection of the full fine grid solution seen in Figure 5.21 onto an 8x8 coarse grid.*

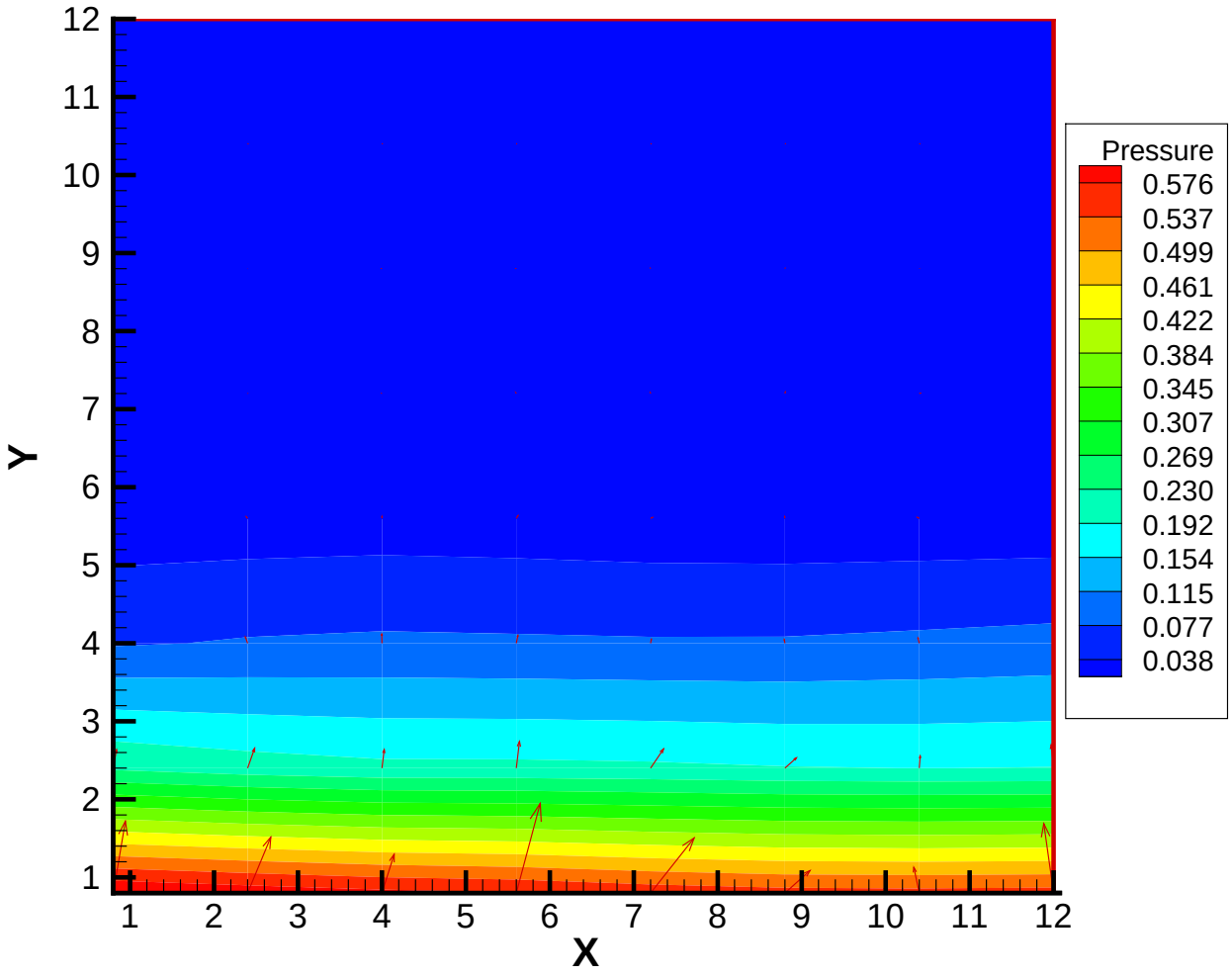

FIG. 5.24. *Example 3, Subcase 3: the upscaled solution from a harmonic-average effective permeability field. The coarse grid is size 8x8.*

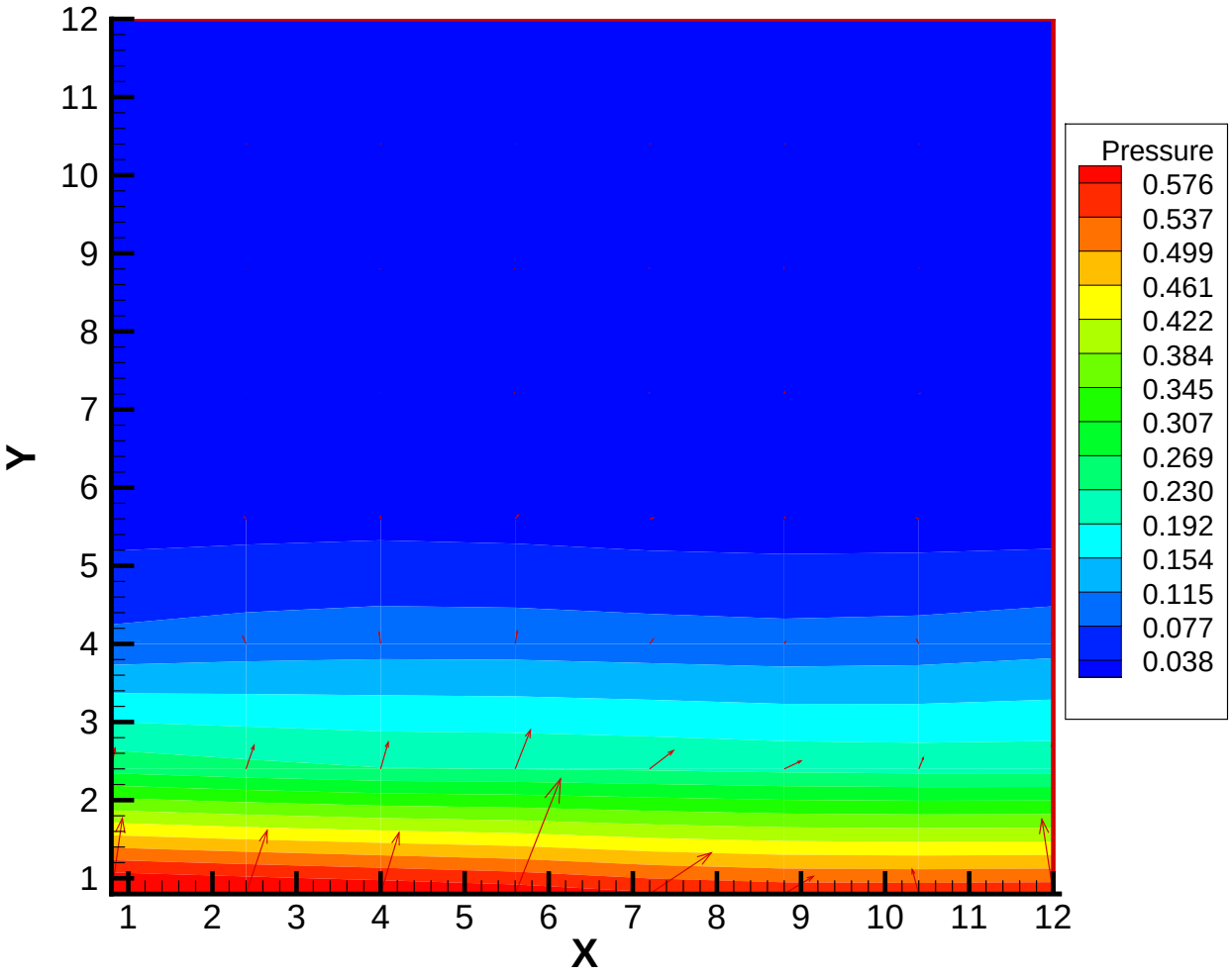

FIG. 5.25. *Example 3, Subcase 3: the upscaled solution from a pressure-solver effective permeability field. The coarse grid is size 8x8.*

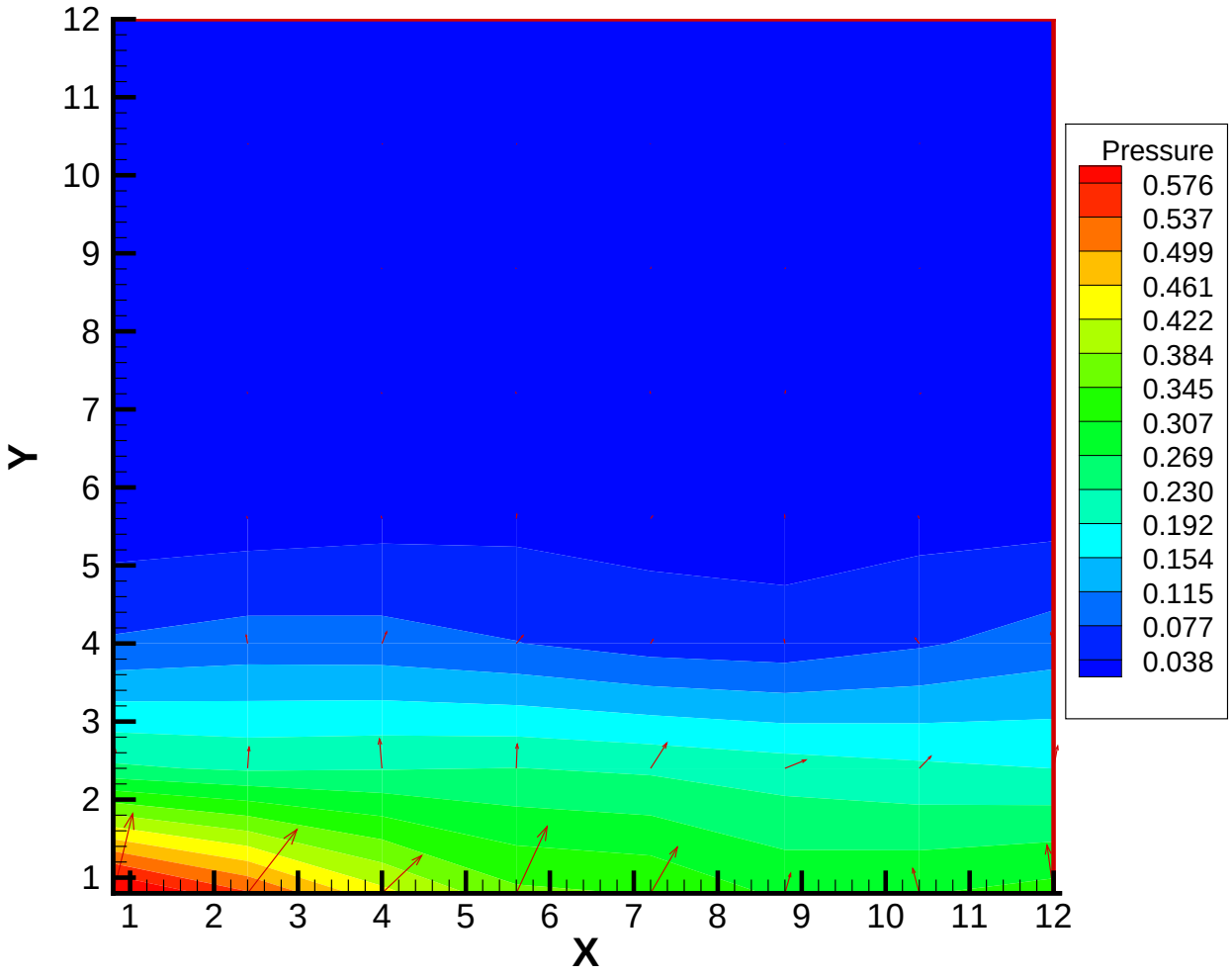

FIG. 5.26. *Example 3, Subcase 3: the operator-based upscaled solution on a coarse grid of size 8x8.*